Geochemistry xxx (xxxx) xxx–xxx

Contents lists available at ScienceDirect

Geochemistry

journal homepage: www.elsevier.com/locate/chemer

Provenance and tectonic setting of the Jurassic Huayacocotla Formation and Alamitos Sandstone, Central Mexico

Yam Zul Ernesto Ocampo-Díaz[a,*], Sonia Alejandra Torres-Sánchez[a], Carita Augustsson[b], José Rafael Barboza-Gudiño[c], José Luis García-Díaz[d], Oscar Talavera-Mendoza[d], Jorge Aceves de Alba[a], Javier Castro-Larragoitia[a], Margarita Martínez-Paco[e], Ricardo Saucedo[c], Alfredo Aguillón-Robles[c]

[a] Área de Ciencias de la Tierra, Facultad de Ingeniería, Universidad Autónoma de San Luís de Potosí, Av. Dr. Manuel Nava No. 8, Zona Universitaria, San Luis Potosí, C.P., 78290, Mexico
[b] Department of Energy Resources, University of Stavanger, 4036 Stavanger, Norway
[c] Instituto de Geología, Universidad Autónoma de San Luis Potosí, Manuel Nava #5Zona Universitaria, San Luis Potosí, S.L.P., Mexico
[d] Unidad Académica de Ciencias de la Tierra, Universidad Autónoma de Guerrero, Ex–Hacienda de San Juan Bautista, S/N, Taxco el Viejo, Guerrero, Mexico
[e] Grupo de Geología Exógena y del Sedimentario, Valle de la Hiedra 113B, Fracc. Valle de Santiago, Soledad de Graciano Sánchez, San Luis Potosí, C.P. 78433, Mexico

ARTICLE INFO

Handling Editor: P.D. Roy

Keywords:
Huayacocotla Formation
Alamitos Sandstone
Sandstone provenance
Geochemistry
Cathodoluminescence
Central Mexico
Climatic change

ABSTRACT

We present a modified model for the paleogeographic evolution of Mexico during Early and Late Jurassic time that is constrained by the tectonic setting and the weathering conditions of the Early Jurassic Huayacocotla Formation and Late Jurassic Alamitos Sandstone basins in state San Luis Potosí in central Mexico. Framework petrography constrains feldspato-quartzose sandstone (mean of $Q_{68}F_{22}L_{10}$) and litho-quartzose (mean of $Q_{75}F_{6}L_{19}$) sandstone compositions for the two units, respectively. The abundant lithic fragments are totally dominated by volcanic fragments. Quartz cathodoluminescence colours and textures from the Alamitos Sandstone supports a large input of volcanic material, but also indicates the presence of metamorphic quartz. Similarly, the geochemical composition is more mafic for the Huayacocotla Formation (Th/Sc: ~0.6 and Cr/Th: ~10) than for the Alamitos Sandstone (Th/Sc: ~1.1 and Cr/Th: ~48). Also the weathering conditions were less intense during the Early (CIA: ~60, PIA: ~61) than the Late Jurassic (CIA ~85, PIA ~97). Well preserved lithic fragments and feldspar grains, particularly in the Huayacocotla Formation, indicate that weathering indeed was minor for this unit. We interpret the difference between the two units as a combined result of climate change and tectonic setting. During the Early Jurassic, transport of volcanic detritus probably dominated from the active Nazas arc in the west. Later, additional sources from the metamorphic basement of Mexico were included. During Late Jurassic time strike-slip faulting related to the opening of the Gulf of Mexico may have re-directed the sediment-transport systems. Finally, the degree of weathering was affected by drastic climatic change from arid to humid tropical conditions during the Middle to Upper Jurassic, possibly related to the first incursions of Gulf of Mexico marine environments linked to the rotation of the Yucatan block.

1. Introduction

Paleogeographical models of the Mexican part of western Pangea are mainly constructed under three main perspectives: (1) the understanding of the geological evolution of the Gulf of Mexico based on the prospects of energy resources (e.g., Pindell, 1985; Pindell and Kennan, 2009), (2) how the establishment and evolution of an Andean-type volcanic arc at the paleo-Pacific margin of Mexico was linked to the opening of the Gulf of Mexico (e.g., García-Díaz, 2004; Barboza-Gudino et al., 2008; 2014; 2015; Rubio-Cisneros and Lawton, 2011), and (3) how the paleo-Pacific and the Atlantic margins of Mexico affected each other (e.g., Ocampo-Díaz, 2011; Barboza-Gudiño et al., 2015; Martini and Ortega-Gutiérrez, 2018). Jurassic oblique subduction towards the east and subsequent roll-back in eastern and central Mexico and rotation of the Yucatan block favored extension. This caused increased exhumation of basement blocks, local climatic changes, and the formation of strike-slip basins (Fig. 1; Rosaz, 1989; Bassett and Busby, 2005; Ocampo-Díaz, 2011; Loyola, 2015; Centeno-García, 2017). The

* Corresponding author.
E-mail address: yamzul.ocampo@uaslp.mx (Y.Z.E. Ocampo-Díaz).

https://doi.org/10.1016/j.chemer.2019.05.004
Received 18 December 2018; Received in revised form 3 May 2019; Accepted 6 May 2019

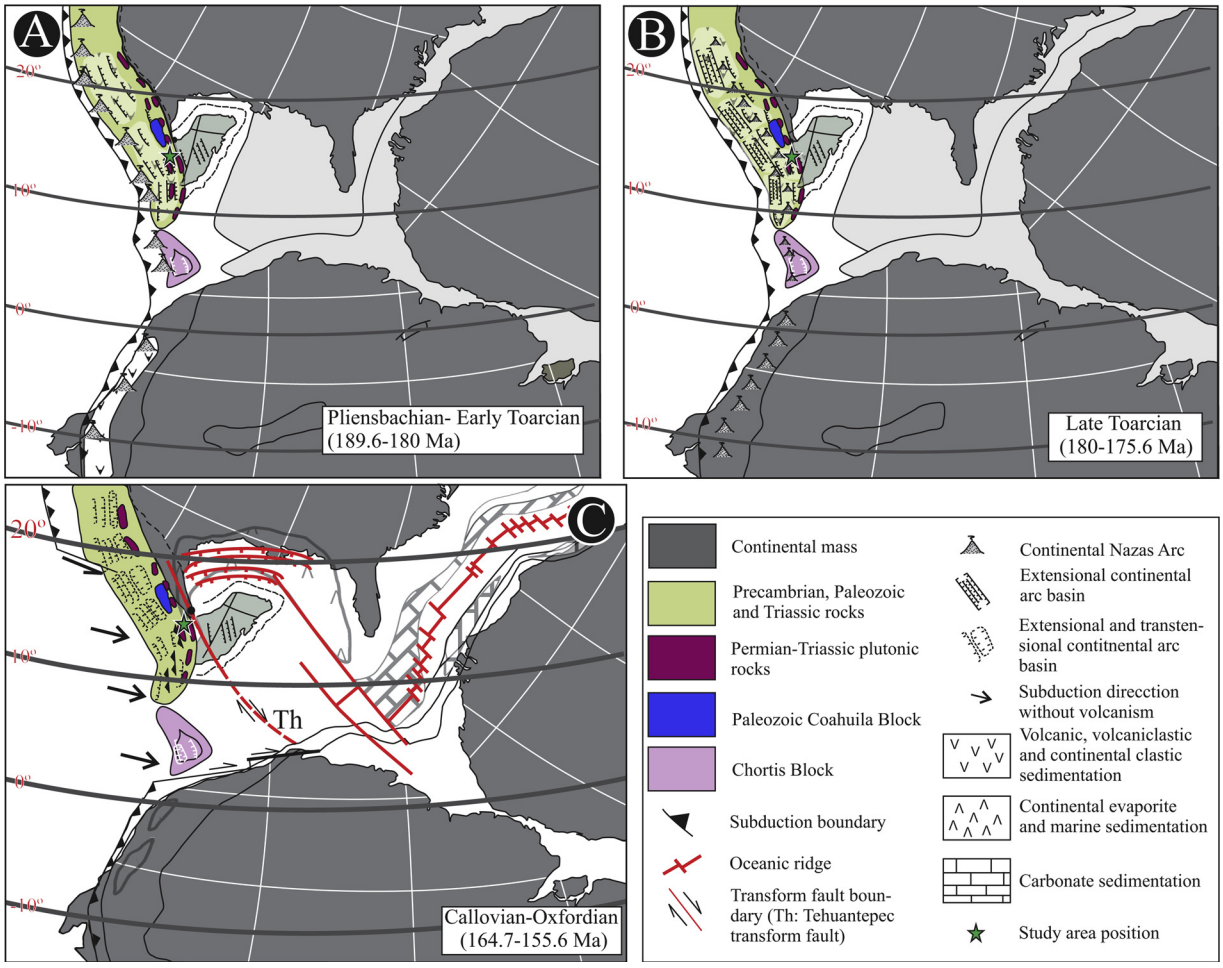

Fig. 1. Jurassic paleogeographic models of Mexico modified from García-Díaz (2004) and Ocampo-Díaz (2011). A): Pliensbachian to Early Toarcian. B): Late Toarcian and C): Callovian to Oxfordian. Green star: location of the study area. Paleogeographic base after Dercourt et al. (1993). (For interpretation of the references to colour in this figure legend, the reader is referred to the web version of this article).

strike-slip basins were situated in continental and marginal-marine environments, filling with clastic sediment that derived from the continental Nazas arc and the metamorphic basement of Mexico (Fig. 1; Barboza-Gudino et al., 2008; 2014; 2015; Rubio-Cisneros and Lawton, 2011). However, the opening of the Gulf of Mexico basin is not well documented, partly because several models invoke an inland rift structure in direct connection with the evolving Pacific margin.

Two alternative tectonic evolution models for Jurassic time have been suggested: 1) Jurassic magmatism in eastern Mexico in the long-lived continental Nazas arc, development of a back-arc basin, and extensional and transtensional continental arc basins. This model also includes Pacific terranes as allocthonous intraoceanic arcs, and the Gulf of Mexico as a rift basin related to the opening of the Atlantic Ocean (Barboza-Gudino et al., 1998, 1999, 2008; 2014; 2015; Ocampo-Díaz, 2011; Ocampo-Díaz and Rubio-Cisneros, 2013; Peña-Alonso et al., 2018). 2) A more complex parautochthonous model includes accretion and supra-subduction rifting with the building of a marginal arc that evolved close to the continent in the paleo-Pacific ocean. Similar to the allochthonous model, the Nazas arc is in a back-arc position, and the Gulf of Mexico is a rift basin related to the opening of the Atlantic Ocean (Elías-Herrera et al., 2000; Centeno-García, 2017;Martini and Ortega-Gutiérrez, 2018).

The main purpose of this work is to re-evaluate the paleogeographic evolution of Mexico during Early and Late Jurassic time. We constrain the tectonic setting of the basin of the siliciclastic Huayacocotla Formation and Alamitos Sandstone deposits in state San Luis Potosí. We do this by combining petrography, geochemistry and cathodoluminescence of quartz for the two units.

2. Geological setting

We here consider the Jurassic tectonic evolution of Mexico following the allochthonous model, because our results indicate that this model is the most plausible one. According to this model, an Andean-type subduction zone with the Farallon plate was established along the paleo-Pacific margin during Early Jurassic time. During the Toarcian (latest Early Jurassic), the subduction slab migrated from west to east towards the Yucatan block (Fig. 1; Ocampo-Díaz, 2011). This resulted in the emplacement of rhyolite, rhyodacite, dacite and andesite of the Nazas and La Boca formations at ca. 190 − 170 Ma, as documented by magmatic zircon (Fastovsky et al., 2005; Barboza-Gudino et al., 2008; Rubio-Cisneros and Lawton, 2011; Lawton and Molina-Garza, 2014) on the Precambrian basement of eastern and northeastern Mexico. A continental and marginal-marine sedimentary system developed in intra-arc, back-arc, extensional and transtensional continental arc basin settings (Fig. 1). The continental La Boca, La Joya, and Todos Santos formations, as well as the deep-marine siliciclastic Huayacocotla Formation were deposited by these systems (Barboza-Gudino et al., 2008, 2014; Venegas-Rodríguez et al., 2009; Godínez-Urban et al., 2011a; Rubio-Cisneros and Lawton, 2011; Ocampo-Díaz, 2011; Ocampo-Díaz and Rubio-Cisneros, 2013). The sedimentary system was fed by detritus from Triassic and older rocks (Venegas-Rodríguez et al., 2009; Godínez-Urban et al., 2011a; Rubio-Cisneros and Lawton, 2011).

The roll-back of the paleo-Pacific slab of the Farallon plate not only

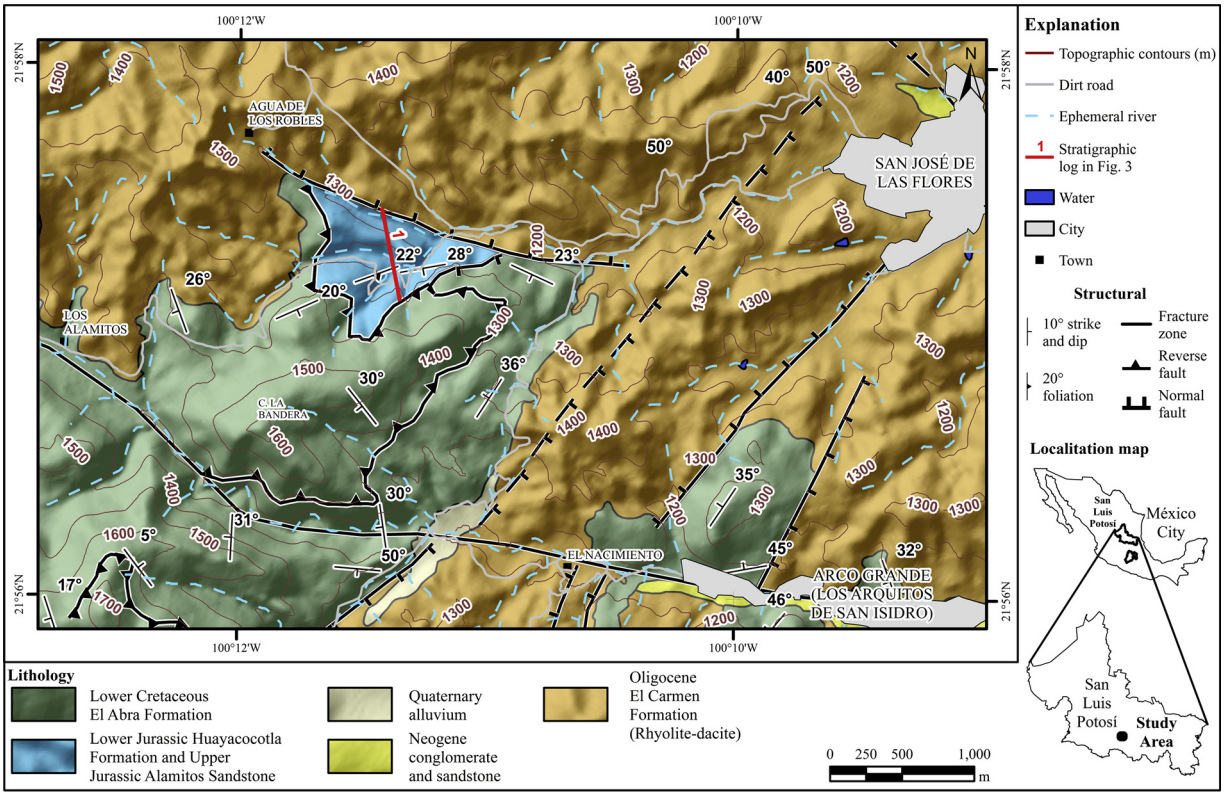

Fig. 2. Geological map of the study area west of San José de la Flores (modified from Labarthe et al., 1989). (For interpretation of the references to colour in this figure legend, the reader is referred to the web version of this article).

triggered the migration of the continental Nazas magmatic arc and the mantle asthenospheric flow, but also favored crustal thinning of the overriding Guerrero plate. This caused exhumation of the Early Jurassic volcanic rocks and older metamorphic basement rocks in an extensional and transtensional continental arc basin during the Middle Jurassic (Fig. 1C; Ocampo-Díaz, 2011; Rubio-Cisneros and Lawton, 2011; Ocampo-Díaz and Rubio-Cisneros, 2013). Meanwhile, the initiation of western Pangea breakup led to the anticlockwise rotation of the Yucatan block on the Atlantic margin side (Pindell, 1985; Dickinson and Lawton, 2001; Pindell and Kennan, 2009; Godínez-Urban et al., 2011a). This caused the development of horst-and-graben systems at the margin of the Gulf of Mexico, as well as continental evaporite sedimentation (Marton, 1995; Dickinson and Lawton, 2001; Fillon, 2007).

During the Late Jurassic, changes in subduction angle of the Farallon plate underneath the Guerrero plate evolved into a high-angle oblique subduction zone that also developed an extensional and transtensional continental arc (*s.s.*, Busby, 2012). The arc was associated with normal and lateral faults that favored exhumation and erosion of the Early to Middle Jurassic volcano-sedimentary successions of the Nazas arc (Fig. 1C; Bassett and Busby, 2005; Ocampo-Díaz, 2011; Ocampo-Díaz and Rubio-Cisneros, 2013; Barboza-Gudiño et al., 2015; Centeno-García, 2017). During the Late Jurassic, the continued opening of the Gulf of Mexico led to left-lateral strike-slip faults, pull–apart and strike–slip basins in Mexico and southern USA (e.g., the Chihuahua and Monterrey troughs; Rosaz, 1989; Goldhammer, 1999; Haenggi, 2002; Bassett and Busby, 2005; Ocampo-Díaz, 2011). Subsequent detachment of the Yucatan Block is linked to the Tehuantepec fault. It caused: a) intense anti-clockwise rotation of ~10° of the Yucatan block (Molina-Garza et al., 1992; Pindell and Kennan, 2009), b) normal faulting of tectonic assemblages at the fringe of the uplifted blocks, and c) continued deposition of continental evaporites in the same area (Marton, 1995; Alaníz-Alvarez et al., 1996; Pindell and Kennan, 2009). Due to the Gulf opening, the Tethys Ocean inundated the continent from the east. This favored peritidal carbonate deposition on the transgressive clastic coastlines (Fig. 1C; e.g., Michalzik and Shumman, 1994; Ocampo-Díaz, 2011; Ocampo-Díaz et al., 2014).

The Jurassic-Cretaceous boundary and Early Cretaceous time were characterized by abrupt changes in sedimentation from clastic to carbonate, a climatic shift from semi-arid to humid tropical conditions, as well as changes in chemical, biotic and tectonic conditions (cf., Adatte et al., 1996; White et al., 2005). The changes were a result of the opened Gulf of Mexico and reactivation of the continental magmatic arcs at the north-western and south-western parts of the paleo-Pacific margin (García-Díaz, 2004; Ocampo-Díaz, 2011). During the Early Cretaceous, the continued rotation of the Yucatan block caused the development of large carbonate platforms on basement highs (e.g., Coahuila, Valles-San Luis Potosí and El Doctor platforms), as well as marginal-marine clastic systems (Winker and Buffler, 1988; Pindell and Kennan, 2009; Ocampo-Díaz, 2011). Simultaneously, the Farallon-plate subduction below the Guerrero plate caused the development of a new continental arc related to the Alisitos-Guerrero subduction system in southwestern USA and southern Mexico (Boschman et al., 2018). In central Mexico a left-lateral transform-fault related continental margin formed. It caused the subduction zone to migrate from northern to southern Mexico (Ocampo-Díaz, 2011; Ocampo-Díaz et al., 2014).

3. Lithostratigraphy of the study area

The Huayacocotla Formation and the Alamitos Sandstone of Toarcian and assumed Oxfordian age (Celestino, 1982; Labarthe et al., 1989; Venegas-Rodríguez et al., 2009) are exposed in San José de las Flores near Río Verde, state San Luis Potosí (Fig. 2). The Huayacocotla Formation consists of a ~60 m-thick unit of rhythmically alternating shale and sandstone turbidites that are arranged in aggradational and progradational successions with well developed compensation cycles (Fig. 3). The sandstone beds are 7–45 cm thick and normally graded (Ta) with upper-plane parallel lamination (Tb), current-ripple marks (Tc), climbing ripples (Tc), and convolute bedding, similar to the "CCC"

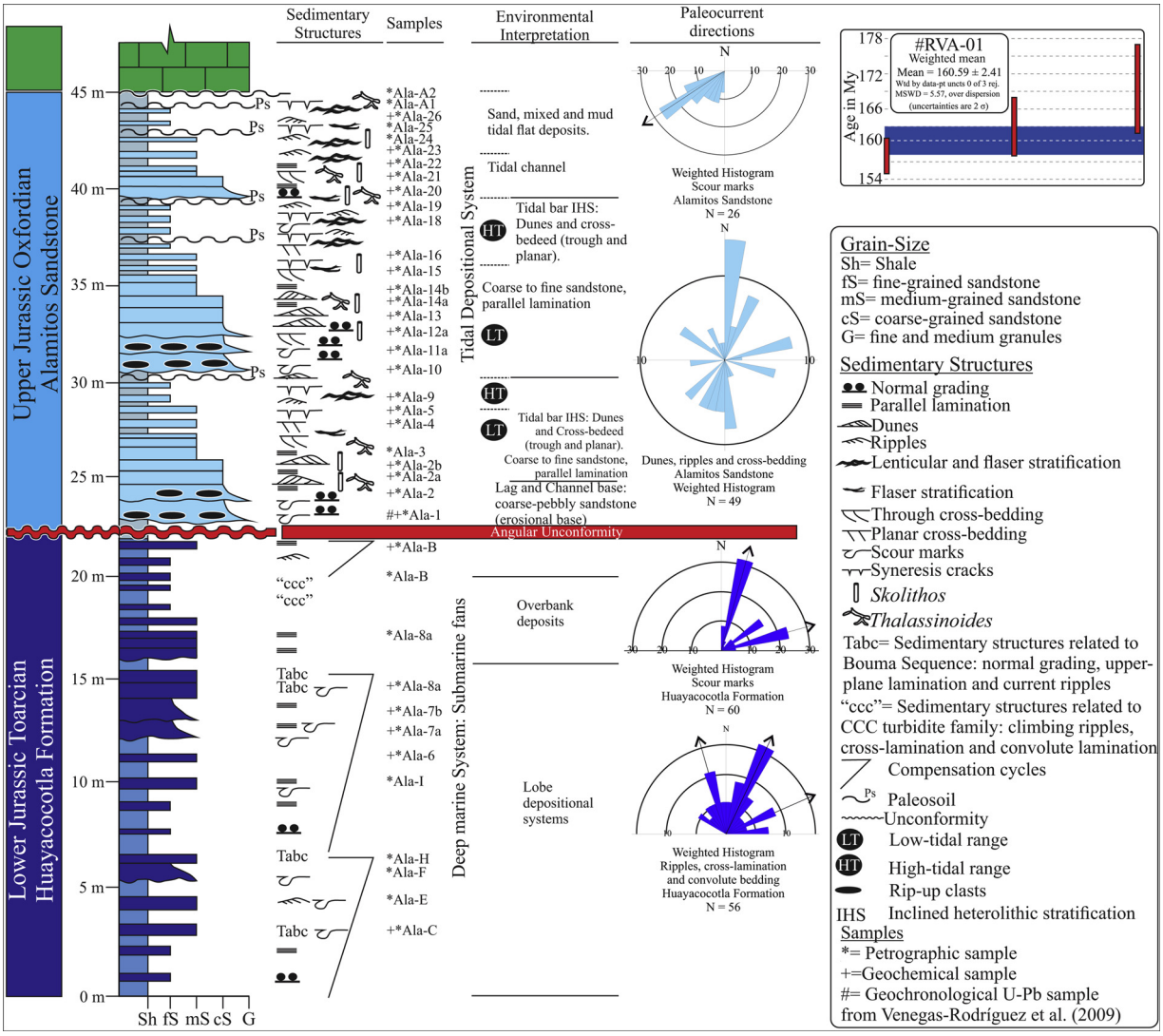

Fig. 3. Sedimentologic log with sedimentological and stratigraphical characteristics of the Huayacocotla Formation and Alamitos Sandstone in the San José de las Flores area. The maximum depositional age from RVA-01 for the Alamitos Sandstone is from Venegas-Rodríguez et al. (2009). (For interpretation of the references to colour in this figure legend, the reader is referred to the web version of this article).

turbidite family of Walker (1992), with erosion grooves and prod-and-skip marks (Fig. 4A-E). The main paleocurrent direction, measured on groove marks, is towards northeast (Fig. 3). The grooves are associated with submarine channel propagation, whereas the current ripples, cross-lamination and convolute bedding are related to lobe progradation and external levees (Fig. 3). The Toarcian age of the Huayacocotla Formation is documented with the ammonites *Phylsecgrammoceras* and *Hidalites* (Labarthe et al., 1989).

The Alamitos Sandstone lies with an angular unconformity on the Huayacocotla Formation (Fig. 4F). The Alamitos Sandstone consists of an aggradational succession of very coarse-grained to fine-grained sandstone with sparse conglomerate beds. The beds vary from 10 to 55 cm in thickness. Common sedimentary bedforms are 3D and 2D dunes with double or single mud-drapes (Figs. 5A-C). They also include inclined heterolithic stratification, through and planar cross-lamination, ripples, lenticular and flaser stratification with bipolar current directions (Fig. 5D). *Skolithos* and *Thalassinoides* trace fossils are present (Fig. 5F), as well as erosional groove-and-scour marks at the base of the bed. Paleosoil and syneresis cracks are common at the upper part of fining-upward successions of the Alamitos Sandstone (Figs. 3, 5F-5 F). The succession is thickening and fining upwards with common rip-up clasts, lags and erosive grooves at the base, along with lenticular bed forms. These characteristics are like the tidal channels documented by Dalrymple (2010). The scour marks and erosive grooves represent tidal channels and suggest sediment transport from northeast to southwest (Fig. 3). The stratification with bipolar current directions is related to tidal sediment transport (Fig. 3). Alamitos Sandstone deposition is bracketed from Oxfordian to Albian based on a maximum depositional age of ~160 Ma (Fig. 3; zircon U-Pb dating, Venegas-Rodríguez et al., 2009), and the overlying Albian El Abra Formation. Celestino (1982) and Labarthe et al. (1989) suggest that the unit is of Late Jurassic age.

4. Methodology

Thin section analysis of 44 medium-grained to coarse-grained sandstone samples were undertaken from seven stratigraphic sections of the Huayacocotla Formation and Alamitos Sandstone collected at the cross-road between the villages of San José de las Flores and Los Alamitos (Figs. 2, and 3). A total of ~1000 grains per sample, excluding matrix and cement, were point-counted with the Gazzi-Zuffa method in order to minimize a modal grain-size effect (Gazzi, 1966; Dickinson, 1970; Zuffa, 1980; Weltje, 2002). Outside the point counting, all lithic fragments larger than 0.0625 mm were described lithologically to reveal their parent rocks. The thin sections were etched with HF and

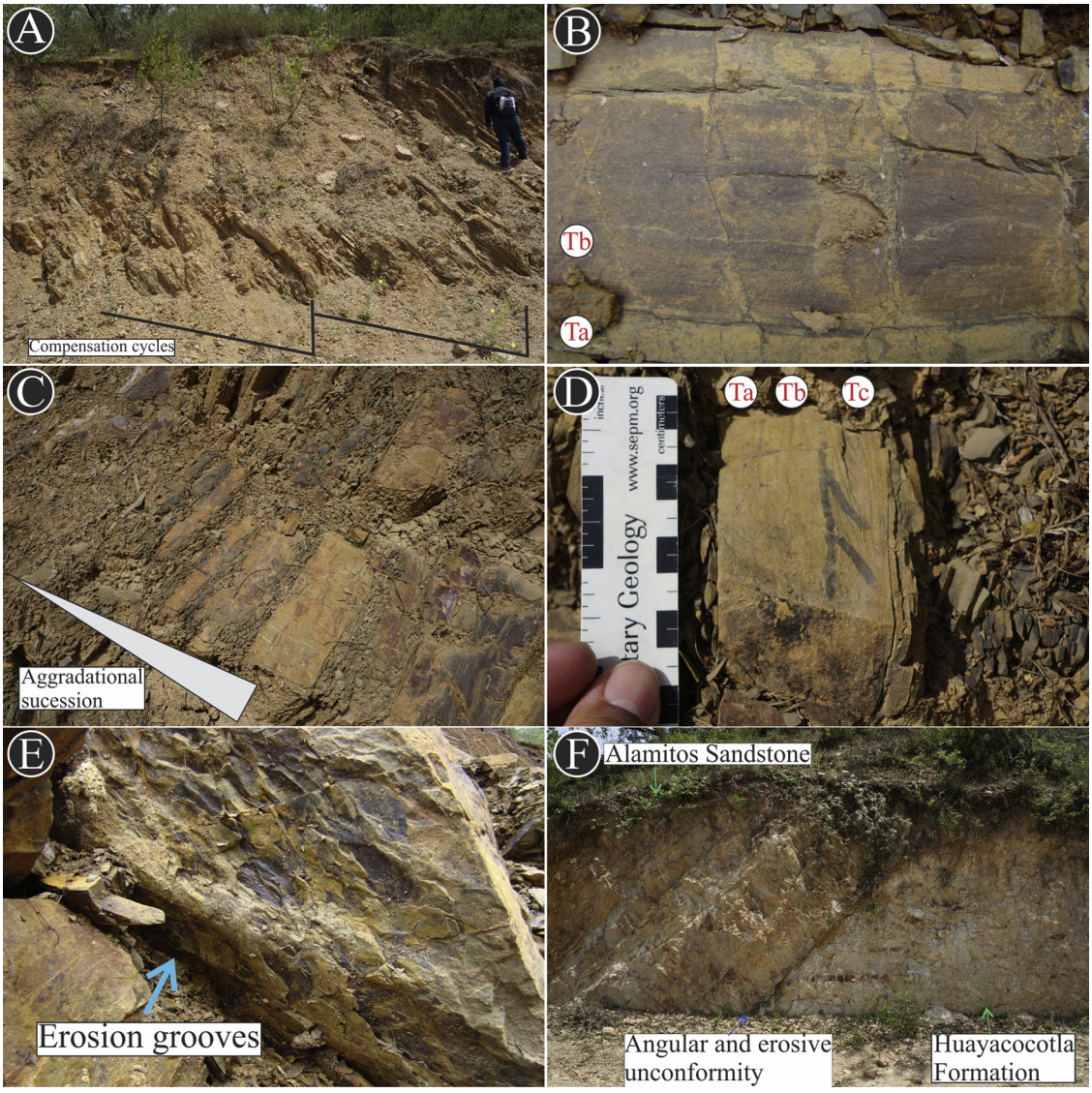

Fig. 4. Field photographs of the Huayacocotla Formation: A) progadational shale-sandstone successions characteristic of depositional lobes. C) aggradational successions of mixed submarine channels. D) Ta, Tb and Tc sedimentary structures of the Bouma sequence. E) Erosion grooves underneath a sandstone bed. F) Angular and erosive unconformity between the Huayacocotla Formation and Alamitos Sandstone.

stained with sodium cobaltinitrite, barium chloride and Alizarin Red for easy recognition of K-feldspar, plagioclase and calcite (Marsaglia and Tazaki, 1992).

Six samples from the Huayacocotla Formation and 20 from the Alamitos Sandstone were analyzed for their whole-rock chemical composition at Acme Labs, Vancouver, Canada. Major and trace elements were analyzed by inductively coupled plasma optical emission spectrometry and inductively coupled plasma mass spectrometry, respectively. The CO_2 values were determined by two-dimensional gas chromatography with a flame ionization detector. The Chemical Index of Alteration (CIA) of Nesbitt and Young (1982), the Index of Compositional Variability (ICV) of Cox et al. (1995), the Plagioclase Index of Alteration (PIA) of Fedo et al. (1995), and the Mafic-Felsic-Weathering (M-F-W) empirical alteration index of Ohta and Arai (2007) were calculated using the formulas CIA = $\{Al_2O_3/(Al_2O_3 + CaO^* + Na_2O + K_2O)\}^*100$; ICV = $(CaO + K_2O + Na_2O + Fe_2O_3 + MgO + MnO + TiO_2)/ Al_2O_3$; PIA = 100 X $(Al_2O_3\text{-}K_2O) / (Al_2O_3 + CaO^* + Na_2O\text{-}K_2O)$; and M = $[-0.395 \times \ln(SiO_2)] + [0.206 \times \ln(TiO_2)] - [0.316 \times \ln(Al_2O_3)] + [0.160 \times \ln(Fe_2O_3)] + [0.246 \times \ln(MgO)] + [0.368 \times \ln(CaO^*)] + [0.073 \times \ln(Na_2O)] - [0.342 \times \ln(K_2O)] + 2.266$. F = $[0.191 \times \ln(SiO_2)] - [0.397 \times \ln(TiO_2)] + [0.020 \times \ln(Al_2O_3)] - [0.375 \times \ln(Fe_2O_3)] - [0.243 \times \ln(MgO)] + [0.079 \times \ln(CaO^*)] + [0.392 \times \ln(Na_2O)] + [0.333 \times \ln(K_2O)] - 0.892$. W = $[0.203 \times \ln(SiO_2)] + [0.191 \times \ln(TiO_2)] + [0.296 \times \ln(Al_2O_3)] + [0.215 \times \ln(Fe_2O_3)] - [0.002 \times \ln(MgO)] - [0.448 \times \ln(CaO^*)] - [0.464 \times \ln(Na_2O)] + [0.008 \times \ln(K_2O)] - 1.374$. CIA is calculated from the molar composition. The Eu anomaly was determining using $Eu/Eu^* = Eu_N/(\sqrt{SmN * GdN})$, where N denotes normalized chondrite values according to Taylor and McLennan (1985).

Colour cathodoluminescence images of detrital quartz from eight samples of the Alamitos Sandstone were made with a Croma Hot CL-II from Gatan mounted to SEM-JEOL at the Universidad Autónoma de Guerrero, Mexico. Images were made selectively to record a variety in cathodoluminescence characteristics during 30 min at 5 mA. Therefore, only qualitative provenance evaluation is done, mainly leaning on the cathodoluminescence texture descriptions of Bernet and Bassett (2005) and Boggs and Krinsley (2006).

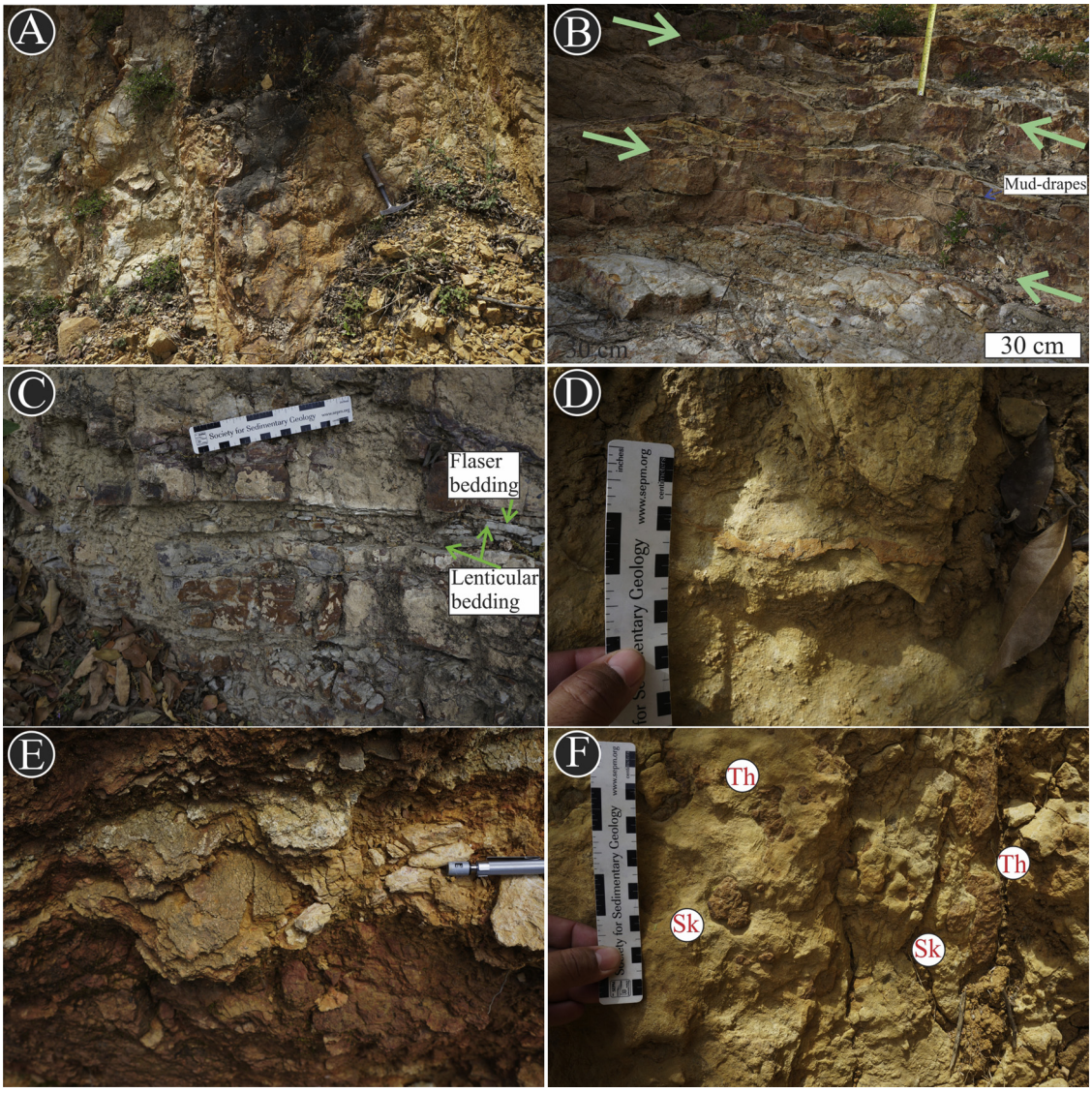

Fig. 5. Field photographs of the Alamitos Sandstone. A) plain view of the 3D dunes. B) cross-section of 3D and 2D dunes with opposite flow direction and double and simple mud-drapes into aggradational succesions. C) Lenticular and flaser stratification. E) Paleosoil. E) Syneresis cracks. F) *Skolithos* and *Thallassinoides* trace fossils.

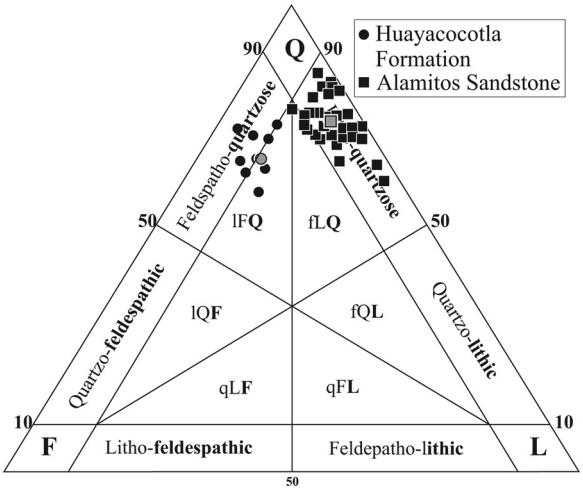

Fig. 6. Framework composition for the studied sandstone units (discrimination fields from Garzanti, 2016). l**FQ**: litho-feldsphato-quartzose; f**LQ**: feldspatho-litho-quartzose; l**QF** litho-quartzo-feldspathic; f**QL**: feldspatho-quartzo-lithic; q**LF**: quartzo-litho-feldspathic; q**FL**: quartzo-feldspatho-lithic.

5. Results

5.1. Petrography

The Huayacocotla Formation sandstone is medium-grained and, compared to much sandstone, fairly poor in quartz and quite rich in feldspar and lithic fragments with mean composition of $Q_{68}F_{22}L_{10}$ (n = 10; Fig. 6). This corresponds to feldspato-quartzose sandstone in the classification of Garzanti (2016). The quartz grains are dominantly subangular to subrounded and monocrystalline (Qm) rather than polycrystalline (Qp; Qp/Qm = 0.01). The monocrystalline quartz grains more commonly are undulatory (Qu) than non-undulatory, i.e., with straight extinction (Qnu; Qnu/Qu = 0.43; Fig. 7A-C; Appendix 1). The monocrystalline grains are characterized by vacuoles, striae and sometimes resorption embayments (Fig. 7B) and syntaxial crystal borders. The polycrystalline quartz grains mostly are composed of elongated crystalline aggregates with sutured, straight or polyhedral subgrain contacts. Plagioclase (P) and alkali feldspar (K) display similar proportions (P/K = 0.9; Appendix 1). The plagioclase grains are slightly sericitized and include albite twins (Fig. 7A-C). The K-feldspar is kaolinized, however Carlsbad and pericline twins are preserved. The lithic grains include volcanic (6%), metapelitic (1) and pelitic rock

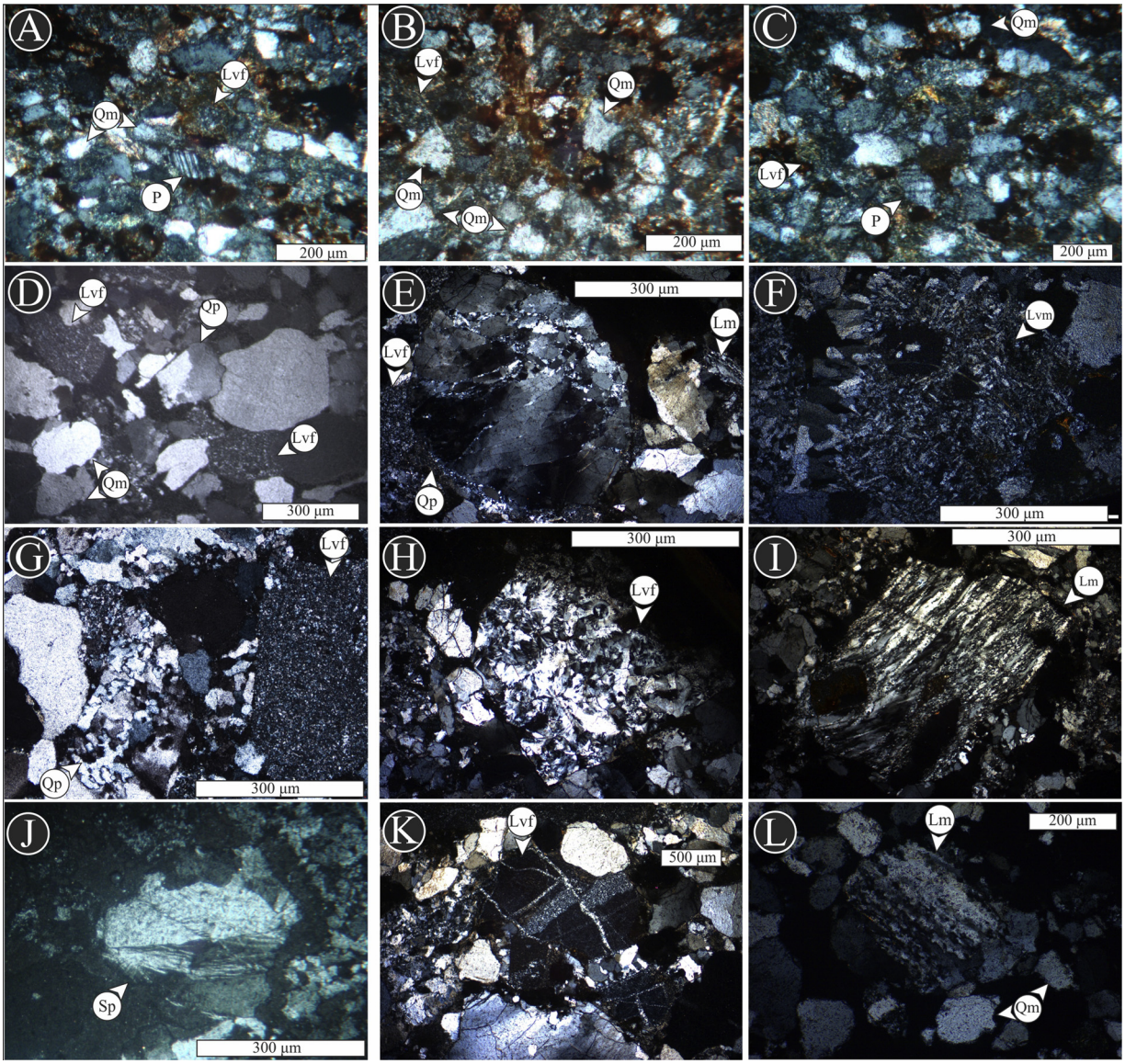

Fig. 7. Microphotographs from Alamitos Sandstones. Microphotographs of the Huayacocotla Formation and Alamitos Sandstone. A, B and C, show the principal petrographic characteristics of the Huayacocotla Formation. Qm-monocrystalline quartz. P-Plagioclase feldspar. Lvf-Felsitic volcanic lithic fragment. D. General petrographic characteristics with monocrystalline quartz (Qm), polycrystalline quartz (Qp) and alkali feldspar (Fk). E. Polycrystalline quartz with more than three subcrystals. F. Microlithic volcanic grain (Lvm). G. Felsitic volcanic grain (Lvf) and polycrystalline quartz. H. Felsitic volcanic lithic fragment. I. Albite llamallae with oxide porphyroblast from metapsammitic lithic fragment. J. Serpentine lithic grain with schistose texture (Sp). L. Felsitic fragment with healed fractures and a fault. L. Low-metamorphic metapelite lithic grain (Lm) and monocrystalline quartz. (For interpretation of the references to colour in this figure legend, the reader is referred to the web version of this article).

fragments (1). The volcanic clasts include (1) felsitic grains with aphanitic texture, sanidine crystals and a chert-like microgranular mosaic of quartz and feldspar, with or without spherulitic chalcedony texture development (Fig. 7B-C), (2) micro-phenocrysts of plagioclase in an aphanitic groundmass that sometimes is vitreous, and; (3) lath-work texture of orthoclase (Appendix 1). Accessory minerals consist of ferrous chlorite, muscovite, epidote, sericite, zircon, and jarosite. Hematite is the most common opaque mineral (Appendix 1). The matrix content is less than 6% and is represented both by true matrix and partly iron-stained pseudomatrix (deformed incompetent lithic fragments). The cement content is less than 5% and mainly consists of calcite sparite.

The Alamitos Sandstone is dominated by medium-grained to coarse-grained sandstone that is slightly more enriched in quartz and lithic fragments than the Huayacocotla Formation with a mean composition of $Q_{75}F_6L_{19}$ (n = 34; Fig. 6; Appendix 1). Monocrystalline quartz is somewhat less common than in the Huayacocotla Formation (Qp/Qm = 0.47) and the monocrystalline quartz grains less commonly exhibit undulatory extinction with Qnu/Qu of 0.56 (Fig. 7D-E). The quartz grains have similar features to those in the Huayacocotla Formation with vacuoles, striae and occasional syntaxial crystal borders (Fig. 7D). In addition, they sometimes contain apatite and zircon inclusions. Different to the Huayacocotla Formation, alkali feldspar dominates completely over plagioclase (P/F = 0.01). It consists of orthoclase and sanidine that sometimes contain carlsbad twins. Some alkali feldspar grains are partly dissolved and corroded or altered to kaolinite. The lithic grains are mainly volcanic (17%), plutonic (observed outside the point-count) and less low-grade to high-grade metamorphic (2%) (Figs. 7F-L). The volcanic grains exhibit (1) felsitic grains with a) equigranular to inequigranular groundmass of quartz and partially chloritized feldspar, b) spherulitic chalcedony and feldspar crystals embedded in a vitreous groundmass, and c) microcrystalline

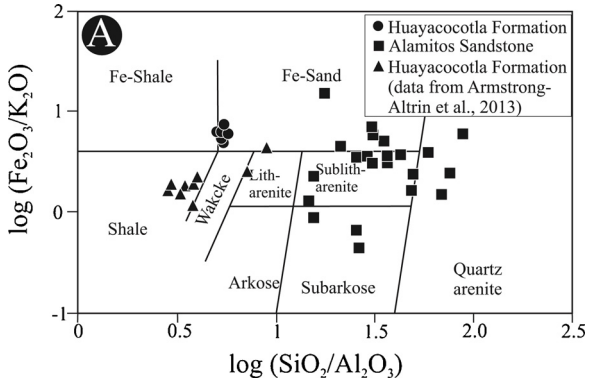

Fig. 8. A) SiO_2/Al_2O_3 vs. Fe_2O3/K_2O. The discrimination lines are after (Herron, 1988). B) K_2O vs. Na_2O. Huayacocotla-Formation data from Armstrong-Altrin et al. (2013) are from Hidalgo state.

quartz and sanidine in a partly altered vitreous groundmass (Figs. 7F, G, H and K); (2) micro-phenocrysts of plagioclase in an aphanitic groundmass; and (3) lathwork of K-feldspar phenocrysts in an aphanitic groundmass that sometimes is vitreous. The plutonic fragments have seriate porphyritic texture and are rich in quartz and feldspar. The metamorphic grains are more common than in the Huayacocotla Formation and consist of metapsammite, metapelite, metabasite and serpentine grain (Figs. 7J and K). Accessory minerals are muscovite, zircon, epidote, baryte, sericite, opaque minerals, biotite, glauconite, chlorite, and apatite. Pseudomatrix, partly replaced by iron oxide, is less than 5%. True matrix is absent. Cement is rare with less than 0.5%. It mainly consists of poikilitic calcite.

5.2. Whole-rock geochemistry

In accordance with the low mineralogical maturity of the Huayacocotla Formation sandstone, the SiO_2 concentration has a mean value of 63%. Other oxide values are relatively high with Al_2O_3 of 12%, Fe_2O_3 of 7%, and K_2O of 1%. As a result, SiO_2/Al_2O_3 and Fe_2O_3/K_2O are approximately 5 and 7, respectively. This corresponds to Fe-sand (Fig. 8), which also is in accordance with the feldspato-quartzose classification. Na_2O/K_2O ratios of 1.9–2.8 are in accordance with the high plagioclase content. The oxide-dependent weathering and alteration indices CIA (Fig. 9a), PIA and ICV are low with mean values of 60, 61 and 1.5, respectively. Values for the empirical alteration index (M-F-W of Ohta and Arai, 2007) are 81 for M, 10 for F and 9 for W (Fig. 9b). In accordance with the high oxide values, the high field strength elements have fairly high absolute concentrations in the Huayacocotla Formation with Zr of 250 ppm, Hf of 7 ppm and Y of 22 ppm. These values also are around or higher than those for the mean upper continental crust (Taylor and McLennan, 1985). Differently, the large ion lithophile elements Rb and Ba have lower values than the upper continental crust (Rb = 40 ppm, Ba = 374 ppm; Appendix 2). The ratio of immobile Th versus mobile U is lower than the upper continental crust with 3. However, ratios of the more immobile and incompatible versus compatible elements Th/Co, La/Co, and Th/Sc indicate a felsic provenance with values that are higher than the upper continental crust with 1, 5, and 0.6, respectively (Fig. 10a). Cr/Ni, Cr/Th, Cr/V, and Ti/Nb, indicators of mafic components, are around or above the values for the upper continental crust with 3, 10, 1, and 433, respectively. Finally, Zr/Sc, which reflects zircon concentration and recycling, is 28, a value that is slightly above that for the upper continental crust (Figs. 10**b;** Appendix 2). The light rare earth elements (LREE) are enriched compared to the heavy ones (HREE) with La_N/Sm_N of 2.8, and Gd_N/Yb_N of 1.8. Eu/Eu* is moderately negative with a mean value of 0.8 (Fig. 11; Appendix 2).

The mineralogically mature sandstone of the Alamitos Sandstone contains more SiO_2 than the Huayacocotla Formation with a mean value of 94%. Correspondingly, other oxide values are lower, which result in higher SiO_2/Al_2O_3 and Fe_2O_3/K_2O of approximately 30 and 10, respectively, corresponding to Fe-sand, litharenite, sub-litharenite, and quartzarenite (Fig. 8). Considering the rare plagioclase in the sandstone, the Na_2O/K_2O of 0.02 − 0.09 is much lower than for the Huayacocotla Formation. Also, different, the Alamitos Sandstone sandstone has high CIA (Fig. 9A), PIA and ICV of 85, 97 and 0.77, respectively, and the values for the empirical alteration index are M = 36, F = 11, and W = 53 (Fig. 9B; Appendix 2). The mobility index Th/U is 4, which is similar to the Huayacocotla Formation. Differently, the felsic indicators Th/Co, La/Co, and Th/Sc are 31, 119, and 1.15, significantly above the values for the upper continental crust. Also, the mafic indicators Cr/Ni, Cr/Th (Fig. 10A), Cr/V, and Ti/Nb, as well as the recycling indicator Zr/Sc (Fig. 10B; Appendix 2), 21, 48, 4, 498, and 73, respectively, are higher than for the Huayacocotla Formation and the upper continental crust (Fig. 11). Similar to the Huayacocotla Formation, the LREE are enriched compared to the HREE with La_N/Sm_N of 4.0 and Gd_N/Yb_N of 1.2 but with a more prominent Eu/Eu*of 0.7 (Fig. 11; Appendix 2).

5.3. Cathodolumenescence of quartz (Alamitos Sandstone)

The cathodoluminescence images reveal that the Alamitos Sandstone is dominated by angular to subangular grains, sometimes with thin quartz-cement rims. Frequently, grains display planar to concavo-convex grain contacts. Much quartz also contains quartz-healed fractures. They occur in all quartz types and often have the same cathodoluminescence colour as quartz cement (Fig. 12A–C), indicating that they are related to brittle deformation due to post-depositional compaction. Six main types of detrital quartz were observed: (1) Quartz with dotted cathodoluminescence appearance. The dots typically are brownish-blue or include different shades of blue (Fig. 12D); (2) bluish quartz grains with microcracks (Fig. 12A); (3) blue-luminescent patchy quartz lacking microcracks (Fig. 12B); (4) dark brownish grains with homogeneous or weakly patchy cathodoluminescence (Fig. 12C); (5) quartz with homogeneous but stronger cathodoluminescence than the brown quartz (Fig. 12E). These grains mostly appear violet and sometimes blue. They contain embayments along grain boundaries or are composed of a single euhedral quartz crystal. (6) Heterogeneous violet to blue or violet to red grains that sometimes include oscillatory zoning also occur (Fig. 12F). Occasionally they include resorption embayments along grain boundaries. Based mostly on images covering numerous grains, the most common types seem to be the dotted (1), the homogeneous violet (5), and zoned quartz (6), as well as homogeneous brown quartz (4).

6. Discussion

We interpret that important compositional differences between the Huayacocotla Formation and the Alamitos Sandstone are due to weathering effects. This is because both units include mafic lithic fragments, both have oxide compositions (M-F-W) indicating mafic input and partly show trace-element compositions being typical for detritus deriving from mafic rock types. This interpretation is supported by the differences in weathering indices, which indicate that the Alamitos Sandstone is more weathered than the Huayacocotla Formation both in San Luis Potosí (this study) and Hidalgo south of our study area (Armstrong-Altrin et al., 2013). In accordance with the CIA and PIA values, differences in weathering are accentuated by the slightly sericitized plagioclase in the Huayacocotla Formation and the presence of altered plagioclase and dissolved potassium feldspar in the Alamitos Sandstone. Feldspar alteration is probably mainly pre-depositional due to the differences in Eu anomaly. Eu/Eu* would be expected to be similar in both units if the difference in feldspar composition would be diagenetic or related to metamorphic source rocks. Due

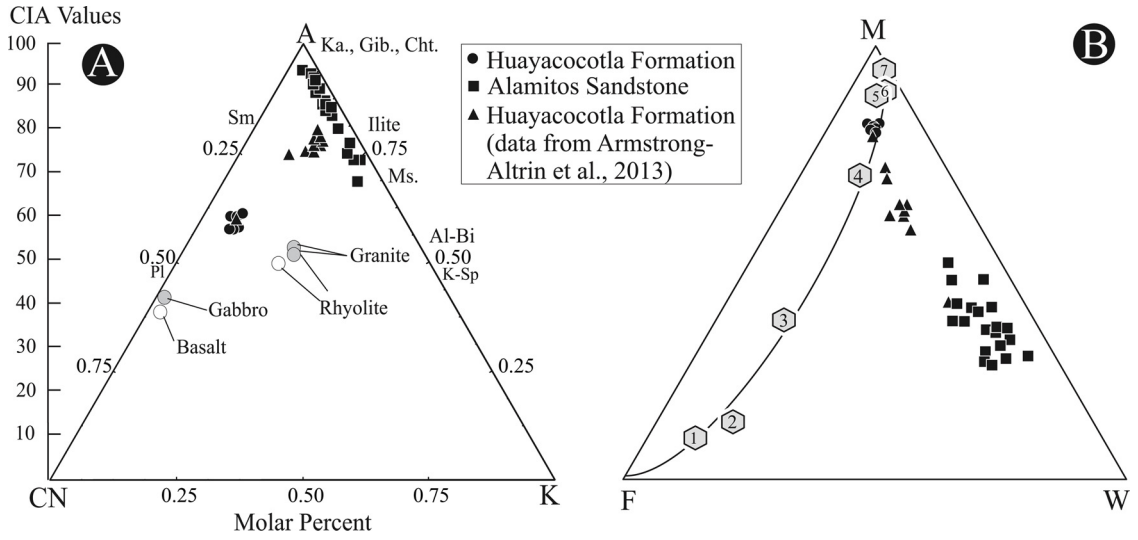

Fig. 9. Weathering diagrams based on oxide concentrations: A) A-CN-K (Al_2O_3 – CaO in silicates only + Na_2O – K_2O) in molar proportions after Nesbitt and Young (1982), and B) Mafic-Felsic-Weathering indices in weight percent according to Ohta and Arai (2007). Chemical composition of granite, rhyolite, basalt and gabbro according to Condie (1993). Ka, kaolinite; Gib, gibbsite; Cht, chlorite; Sm, smectite; Ms, muscovite; K-sp, K-felsdpar; Pl, Plagioclase, Al-Bi, Alkaline Biotite. Numbers in Fig. 6b are: 1, calc-alkali rhyolite; 2, granite; 3, calc-alkali dacite; 4, calc-alkali andesite; 5, volcanic-arc basalt; 6, alkali basalt; 7, komatiite.

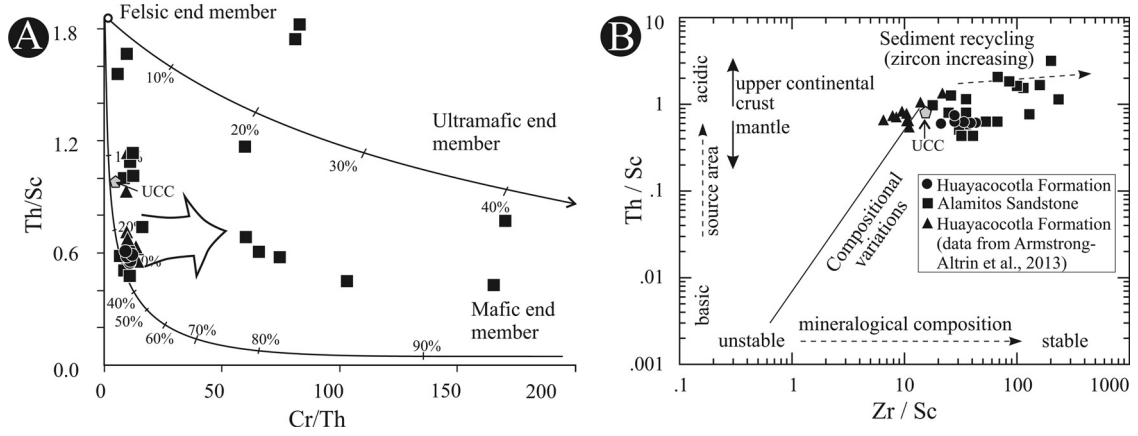

Fig. 10. A) Cr/Th versus Th/Sc for determining mafic and ultramafic source rocks. B) Zr/Sc versus Th/Sc for determining sedimentary recycling process and source rocks evolution. The discrimination lines are from Condie and Wronkiewiez (1990) and McLennan et al. (1993).

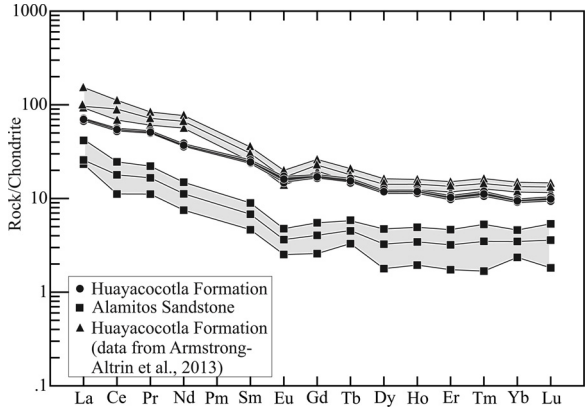

Fig. 11. Chondrite-normalized rare earth element concentrations (chrondrite values from Taylor and McLennan, 1985).

the position of the depositional basin between the continental Nazas arc and the rifting Gulf of Mexico, the transport distance for both the Huayacocotla Formation and the Alamitos Sandstone is expected to be rather short. Therefore, the difference in composition cannot be explained solely by long transport (both in distance and time) over extended continental areas.

The weak weathering in the Huayacocotla Formation probably is mainly due to erosion and transport in an arid climate into the topographic lows - with high similarities to the Huayacocotla Formation in Hidalgo (Armstrong-Altrin et al., 2013). The stronger weathering conditions for the Alamitos Sandstone are in accordance with a more humid climate. Also a topographic change from high to low relief could have explained our results. However literature data indicate that a climate change indeed took place during this time. Based on palynological and stable isotope analysis on Jurassic red beds in central and northeastern Mexico, Loyola (2015) postulated a warm-arid climate during Early Jurassic time and warm-humid subtropical to tropical conditions during Middle to Upper Jurassic time. Similarly, Korte et al. (2015) proposed a global climate change from warm conditions during the Toarcian, to cooler temperatures for the Middle and Late Jurassic. This change is related to lithospheric up-doming and uplift in the North Sea, impeding heat transport and thus triggering cooler conditions (Korte et al., 2015).

The difference in weathering due to climate was probably accentuated by a difference in transport distance, possibly combined with differences in relief. This is based on the dominance of volcanic lithic

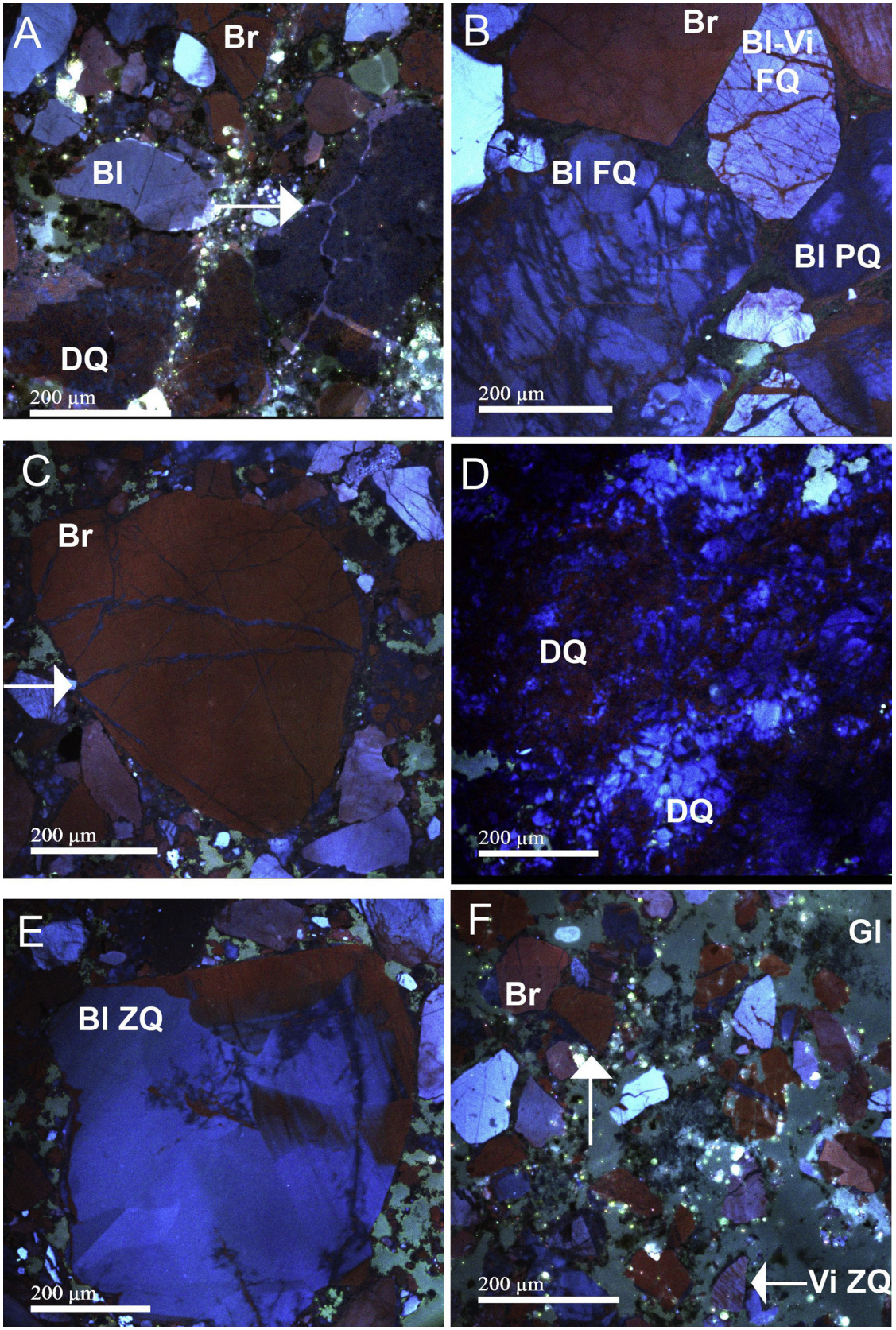

Fig. 12. CL images of quartz. A. Blue-brown dotted quartz (DQ), blue (Bl) and brown (Br) luminescent quartz. The arrow marks a quartz-healed fracture (sample Ala-B). B. Brown (Br) quartz, fractured quartz (FQ) of blue (Bl) and blue-violet (Bl-Vi) luminescence, and blue patchy quartz (Bl PQ; sample Ala-5). C. Brown (Br) fractured quartz. The arrow marks a fracture. Note the thin quartz-cement rim of the same colour shade (sample Ala-12). D. Blue and blue-brown dotted quartz (DQ; sample Ala-22). E. Blue zoned quartz (Bl ZQ; sample Ala-12). F. A variety of quartz grains of different colour shades, including brown (Br) and violet zoned quartz (Vi ZQ; sample Ala-B). The brightest blue grains are feldspar. Gl = thin-section glass. (For interpretation of the references to colour in this figure legend, the reader is referred to the web version of this article).

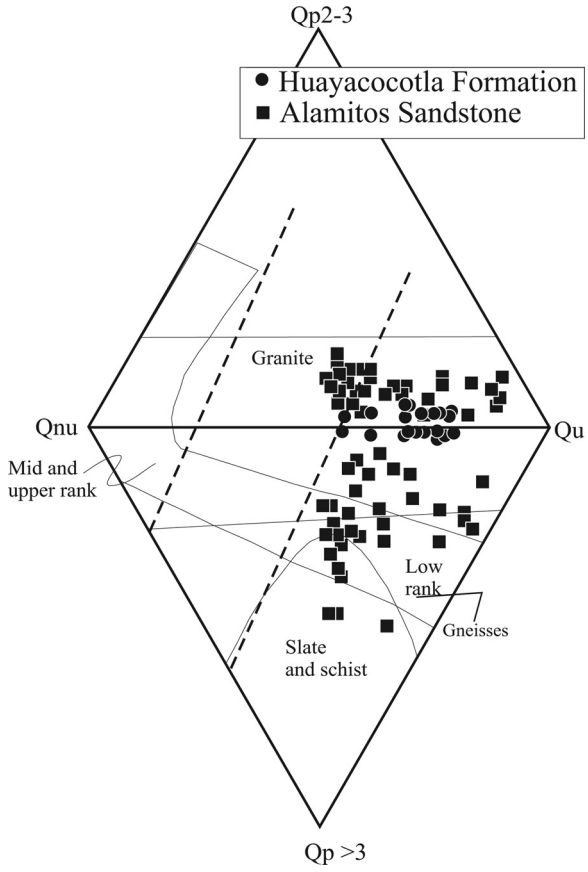

Fig. 13. Quartz types in sandstone (discrimination lines from Basu et al., 1975 (dashed lines) and Tortosa et al., 1991 (solid lines). Qnu-nonundulatory monocrystalline quartz; Qu-undulatory monocristalline quartz; Qp2-3-polycrystalline quartz grains with 2 or 3 subcrystals; Qp > 3-polycrystalline quartz grains with more than 3 subcrystals (excluding chert).

fragments in the Huayacocotala Formation and the more varied lithograin content of volcanic fragments mixed with plutonic and metamorphic clasts in the Alamitos Sandstone sandstone that may indicate that the Huayacocotla Formation basin was situated closer to the paleo-Pacific convergent margin and the Nazas arc than the Alamitos Sandstone basin. However, during Late Jurassic time, the assumed age of the mature Alamitos Sandstone, rifting related to the Gulf of Mexico was more pronounced than earlier (Ocampo-Díaz, 2011). This caused locally different tectonic settings in the area between the Pacific and Atlantic oceans, and different microclimates were also possible. The postulated climate change in the Huayacocotla-Formation and Alamitos-Sandstone basins and in central and northeastern Mexico may have been favored by the regional strike-slip fault systems that exhumed basement rocks. This process interfered with the heat transport and led to a tropical climate with humid conditions (cf., Gose et al., 1982; Loyola, 2015; Korte et al., 2015). The central Mexican paleoposition both during Early and Late Jurassic time is estimated to approximately 24 °N (Gose et al., 1982; Pindell and Kennan, 2009). This agrees with paleomagnetic data of 2–6 °N for the southwestern part of the Yucatan block (Lower Jurassic La Silla Formation and Middle Jurassic Todos los Santos Formation; Godínez-Urban et al. (2011b). Hence plate movements cannot explain the change in climate.

7. Provenance

The volcanic lithic fragments indicate that volcanic rocks were the main source for both units. The large influence of volcanic sources is accentuated by the dominance of violet-luminescent and zoned quartz grains in the Alamitos Sandstone, both of which is typical for volcanic quartz (Augustsson and Reker, 2012). Also, the resorption embayments and the lack of microfractures in the quartz indicate volcanic sources (Bernet and Bassett, 2005; Boggs and Krinsley, 2006). Additionally, the grains with dotted cathodoluminescence appearance are similar to felsic volcanic groundmass that was illustrated by Augustsson and Reker (2012). This also is in accordance with the presence of lithic clasts with felsic volcanic groundmass in both units. Both the felsic volcanic grains and quartz, and the mafic petrographic and geochemical indicators suggest a similar but varied volcanic source for the two units. The volcanic source may include rhyolitic to andesitic lava from the continental Nazas Arc directly to the west of our study area. This is supported by detrital zircon ages for the Alamitos Sandstone that are in accordance with ages from the Nazas Arc (Fig. 14; Venegas-Rodriguez et al., 2009).

Besides the volcanic input, lithological catchment-area differences are recorded in the sedimentary clasts of the Huayacocotla Formation, and the felsic plutonic lithic fragments of the Alamitos Sandstone. Plutonic quartz also is indicated by the usually blue-luminescent quartz with microcracks (cf. Bernet and Bassett, 2005). Furthermore, the much higher immobile element ratios Th/Co, La/Co, and Th/Sc indicate more felsic sources for the Alamitos Sandstone than the Huayacocotla Formation (cf. Bhatia and Crook, 1986). The metasedimentary lithic fragments and the larger proportion of polycrystalline than monocrystalline quartz in the Alamitos Sandstone also indicate a stronger influence from low-grade to medium-grade metamorphic sources influenced by < 500 °C (cf. Basu et al., 1975; Tortosa et al., 1991; Figs. 13 and 14). This is supported by the frequent brown-luminescent quartz, because both the weak cathodoluminescence signal and the patchy texture are typical for metamorphic quartz formed at temperatures from 300 to 350 °C up to ca. 500 °C (Zinkernagel, 1978; Boggs and Krinsley, 2006; Augustsson and Reker, 2012).

In agreement with the petrographic differences for the two units, the low and high ratios, respectively, for the incompatible versus compatible element ratios Th/Co, La/Co, and Th/Sc in combination with the recycling indicator Zr/Sc are typical for continental island arcs for the Huayacocotla Formation both in the study area and in Hidalgo region (cf., Armstrong-Altrin et al., 2013), and for passive margin for the Alamitos Sandstone (cf. Bhatia and Crook, 1986). Nevertheless, the large amount of lithic fragments in the Alamitos Sandstone and the dominance of volcanic clasts among these are untypical for passive margins (cf. Dickinson and Suczek, 1979). Together with the plutonic clasts in the Alamitos Sandstone, this indicates that both studied units may partly have been sourced from areas that are related to an active or passive igneous arc. If the arc was active, the volcanic arc may have migrated towards the west during late Middle to early Late Jurassic time (Ocampo-Díaz, 2011; Cruz-Gámez et al., 2017). In that case, we assume that the migration opened up for more varied source lithologies for the younger Alamitos Sandstone (Fig. 14).

The Huayacocotla Formation sand probably mainly derived directly from the exhumed continental Nazas Arc located west of the study area. In the eastern, the right-lateral opening of the Gulf of Mexico caused exhumation of basement rocks in a horst-and-graben landscape, which may be the source for the metapelitic rock fragments. Particularly, the westernmost metapelite occurrences of the Paleozoic Granjeno Schist (Barboza-Gudiño et al., 2011) are a potential source candidate (Fig. 14).

Similar to the Huayacocotla Formation, the felsic composition of the Alamitos Sandstone can be explained by basement uplift and erosion (Fig. 14; Venegas-Rodríguez et al., 2009). However, the opened Gulf of Mexico in the east caused both further graben basins and the first oceanic transgression from the Gulf into northeastern and central Mexico (e. g., Ocampo-Díaz, 2011; Centeno-García, 2017; Martini and Ortega-Gutiérrez, 2018; Fig. 15). We propose that the shallow-marine Alamitos Sandstone represents the coastal area of the early Gulf of Mexico (Fig. 15B). Due to the continued extension, the Nazas Arc may have been exhumed further with the potential for arc material of the

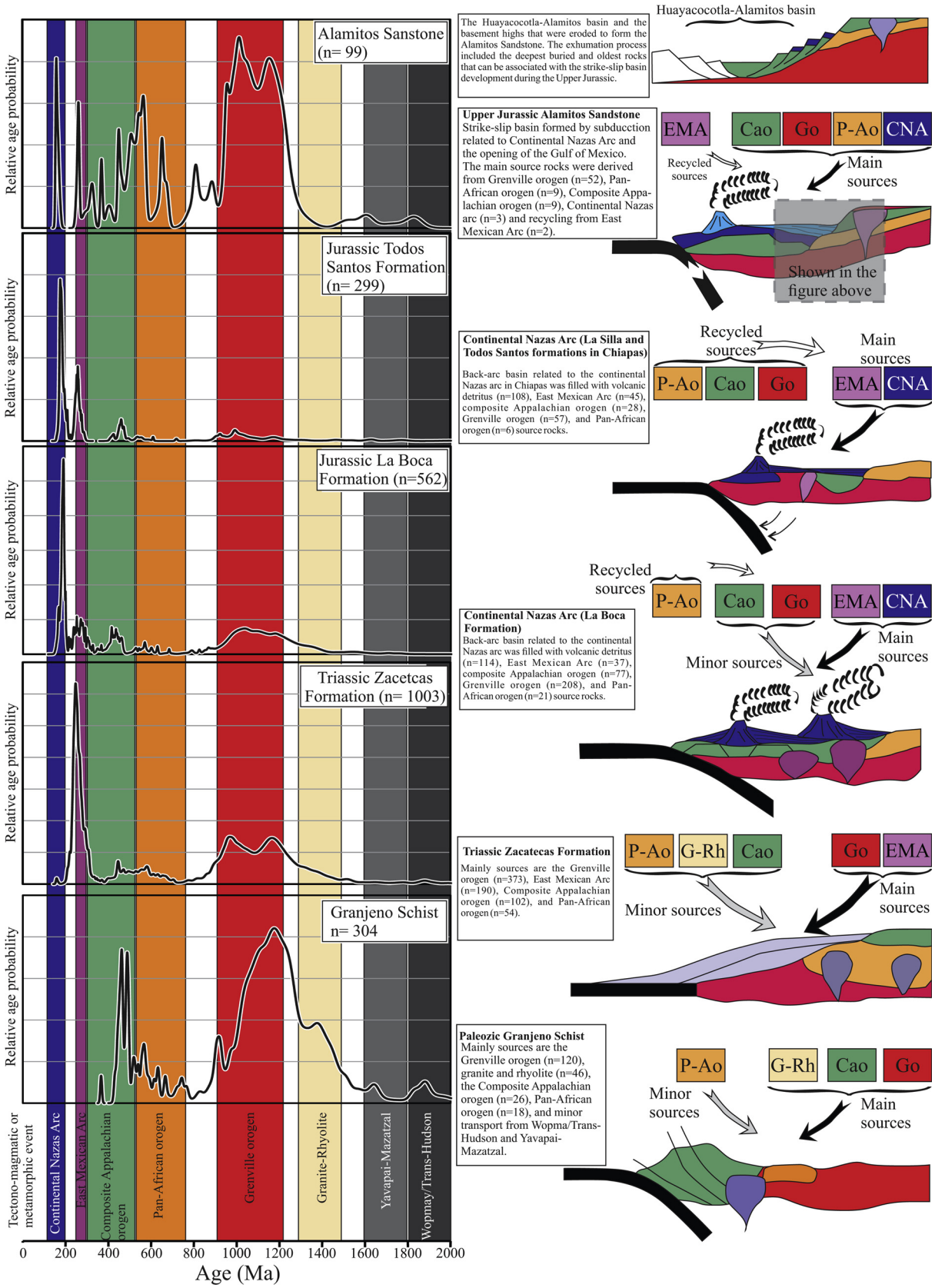

Fig. 14. Tectonic evolution and probability densities of detrital zircon ages for the Paleozoic Granjeno Schist, Triassic Zacatecas Formation, Lower Jurassic La Boca Formation, Lower and Middle Jurassic La Silla and Todos Santos formations, and Upper Jurassic Alamitos Sandstone. The color bands represent expected ages of Mexican source rocks, particularly ages of magmatic and metamorphic events on the west edge of Mexico according to Lawton et al. (2016). The zircon data are from Venegas-Rodríguez et al. (2009); Barboza-Gudiño et al. (2010, 2011); Rubio-Cisneros and Lawton (2011); Godínez-Urban et al. (2011a); Barboza-Gudiño (2012), and Ortega-Flores et al. (2014, 2016). Abbreviations are: Go, Grenville Orogen; Cao, Composite Appalachian Orogen; G-Rh, Granite-Rhyolite; P-Ao, Pan-African orogen; EMA, East Mexican Arc; CAN, Continental Nazas Arc. (For interpretation of the references to colour in this figure legend, the reader is referred to the web version of this article).

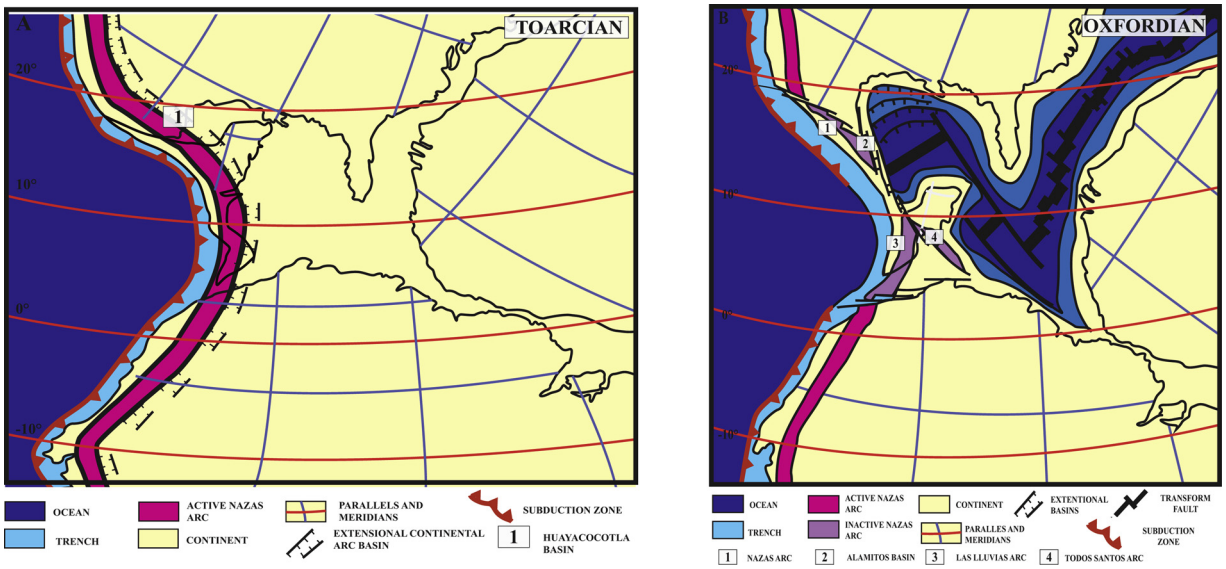

Fig. 15. Proposed paleogeographic configuration from Mexico during Toarcian (A) and Oxfordian (B). The paleogeographic base is modified from Coney (1983); García-Díaz (2004) and Ocampo-Díaz (2011). (For interpretation of the references to colour in this figure legend, the reader is referred to the web version of this article).

same composition and age to be the source for the Huayacocotla Formation and the Alamitos Sandstone (Figs. 14, and 15). Also, basement rocks probably continued being exhumed further with continuous erosion of the Granjeno Schist as well as the more felsic Novillo Gneiss (Fig. 14). In addition to metapelite, the Granjeno Schist also includes metapsammite and mafic to ultramafic metavolcanic rocks, including serpentinite (Barboza-Gudiño et al., 2011; Torres-Sánchez et al., 2017). We propose that the Granjeno Schist, with estimated metamorphic temperatures around 300 °C (Torres Sánchez et al., 2016, 2017) was exhumed to its metapsammitic and metavolcanic rocks by Late Jurassic time (Fig. 14). This can explain the varied metasedimentary lithic clast content, the more abundant polycrystalline quartz, the low-temperature quartz as well as the metabasite and serpentinite fragments in the Alamitos Sandstone (Fig. 14). Detrital input from Granjeno-Schist serpentinite that contains 1–5 weight % Cr_2O_3 (Torres-Sánchez et al., 2017) also explains the high Cr/Ni, Cr/Th and Cr/V, that seemingly cause a contrasting felsic-mafic geochemical signal together with the high La/Co, Th/Co, and Th/Sc for the Alamitos Sandstone. Also, the enrichment of HREE compared to the upper continental crust and the oxide-dependent mafic value for the empirical alteration index M-F-W can be due to the serpentinite clasts (Lesnov, 2010).

A potential source for the felsic plutonic lithic fragments and plutonic quartz can be the ca. 1.0–1.2 Ga Novillo Gneiss (Weber et al., 2010), which is mainly composed of metagranitoid, metagabbro, and calcsilicate at granulite-facies metamorphism (Ortega-Gutiérrez et al., 2018). This interpretation is valid since crystal borders commonly are similar in plutonic and high-temperature metamorphic rocks (e. g., Götze and Zimmerle, 2000). Also, the cathodoluminescence signal is similar for plutonic quartz and metamorphic quartz above ca. 500 °C (Augustsson and Reker, 2012). Furthermore, ca. 1 Ga zircon grains are present in the Alamitos Sandstone (Fig. 14; Venegas-Rodröguez et al., 2009).

Different to our model, traditionally the Huayacocotla Formation and Alamitos Sandstone have been interpreted as basin deposits along a passive continental margin that was associated with the opening of the Gulf of Mexico (e. g., Armstrong-Altrin et al., 2013). However, our tectonic interpretation is in accordance with Venegas-Rodríguez et al. (2009); Ocampo-Díaz (2011), and Barboza-Gudino et al. (2010, 2015), who suggested that the Lower Jurassic Huayacocotla Formation has a closeness with an active continental margin along the paleo-Pacific margin of Mexico (Fig. 15A), whereas the Upper Jurassic Alamitos Sandstone is linked to the first incursion of the Gulf of Mexico, which at the same time is associated with a strike-slip basin system that developed due to Yucatan block rotation and the oblique subduction of the paleo-Pacific Farallon plate (Ocampo-Díaz, 2011; Barboza-Gudiño et al., 2014; Fig. 15B). This interpretation agrees with active sinistral movement in a sedimentary basin in southern Mexico during Middle Jurassic time (Tezoatlán basin *sensu* Zepeda-Martínez et al., 2018).

8. Conclusions

The provenance results indicate two different sources for the Huayacocotla Formation: 1) the Early Jurassic Continental Nazas arc that bounded the Huayacocotla-Formation and Alamitos-Sandstone basins to the north and east, and 2) minor input from uncovered low-grade, partly mafic, metamorphic rocks of the Granjeno Schist. Sources for the overlying Alamitos Sandstone included 1) Precambrian and Paleozoic metaigneous, metasedimentary and ultramafic rocks from the Novillo Gneiss and the Granjeno Schist, and 2) volcanic rocks from the Nazas Arc. This provenance change is related to the exhumation of crystalline basement in Tamaulipas north of the study area along left-lateral strike-slip fault systems. The depositional basins are part of the span of strike-slip basins that extended from north-central to south-eastern Mexico during the Upper Jurassic to Lower Cretaceous (Ocampo-Díaz, 2011; Ocampo-Díaz et al., 2014). The data from the present study, in addition to those from previous authors, strengthen the suggestion for a provenance shift from an active continental margin during the Lower Jurassic, to a system that involves the last stage of an active margin with lateral fault systems associated with the Gulf of Mexico opening. These evolving tectonic regimes favored climate changes that were related to the exhumation of basement highs and the marine incursion of the Gulf of Mexico.

Funding

Support for this study was received from the CONACYT Ciencia Básica projects 2012-101548, 2011-169231 and PRODEP project 511-6/17-7930.

Acknowledgments

Thanks to María Guadalupe López Martínez for help by the stained

thin-section, and Jazmín López Díaz for her assistance on the CL-images capture. The authors acknowledge Martin Guerrero-Suastegui for his comments and Paul Nadeau for English corrections. We want to thank to the two anonymous reviewers for their constructive suggestions and comments which have significantly improved the manuscript.

Appendix A. Supplementary data

Supplementary material related to this article can be found, in the online version, at doi:https://doi.org/10.1016/j.chemer.2019.05.004.

References

Adatte, T., Stinnesbeck, W., Remane, J., Hubberten, H., 1996. Paleoceanographic changes at the Jurassic-Cretaceous boundary in the Western Tethys, northeast Mexico. Cretac. Res. 17, 671–689. https://doi.org/10.1006/cres.1996.0036.

Alaníz-Alvarez, S.A., van der Heyden, P., Samaniego, A.F.N., Ortega-Gutiérrez, F., 1996. Radiometric and kinematic evidence for Middle Jurassic strike-slip faulting in southern Mexico related to the opening of the Gulf of Mexico. Geology 24, 443–446. https://doi.org/10.1130/0091-7613(1996)024.

Armstrong-Altrin, J.S., Nagarajan, R., Madhavaraju, J., Rosales-Hoz, L., Lee, Y.I., Balaram, V., Cruz-Martínez, A., Avila-Ramírez, G., 2013. Geochemistry of the Jurassic and Upper Cretaceous shales from the Molango Region, Hidalgo, eastern Mexico: Implication for source-area weathering, provenance, and tectonic setting. Comptes Rendus Geosci. 345, 185–202. https://doi.org/10.1016/j.crte.2013.03.004.

Augustsson, C., Reker, A., 2012. Cathodoluminescence spectra of quartz as provenance indicators revisited. J. Sediment. Res. 82, 559–570. https://doi.org/10.2110/jsr.2012.51.

Barboza-Gudiño, J.R., 2012. Sedimentary tectonics and stratigraphy: the early mesozoic record in central to northeastern Mexico. In: Elitok, Ö. (Ed.), Stratigraphic Analysis of Layered Deposits. InTech., pp. 255–278.

Barboza-Gudino, J.R., Tristán-González, M., Torres-Hernández, J.R., 1998. The Late Triassic-Early Jurassic active continental margin of western North America in northeastern Mexico. Geofísica Internacional 37 (4), 283–292.

Barboza-Gudino, J.R., Tristán-González, M., Torres-Hernández, J.R., 1999. Tectonic setting of pre-Oxfordian units from central and northeastern Mexico: a review. Geol. Soc. Am. Spec. Pap. 340, 197–210. https://doi.org/10.1130/0-8137-2340-X.197.

Barboza-Gudino, J.R., Orozco-Esquivel, M.T., Gómez-Anguiano, M., Zavala-Monsiváis, A., 2008. The Early Mesozoic volcanic arc of western North America in northeastern Mexico. J. South Am. Earth Sci. 25, 49–63. https://doi.org/10.1016/j.jsames.2007.08.003.

Barboza-Gudiño, J.R., Zavala-Monsiváis, A., Venegas-Rodríguez, G., Barajas-Nigoche, L.D., 2010. Late Triassic stratigraphy and facies from northeastern Mexico: tectonic setting and provenance. Geosphere 6, 621–640. https://doi.org/10.1130/GES00545.1.

Barboza-Gudiño, J.R., Ramírez-Fernández, J.A., Torres-Sánchez, S.A., Valencia, V., 2011. Geocronología de circones detríticos del Esquisto Granjeno en el noreste de México: implicaciones tectónicas. Boletín de la Sociedad Geológica Mexicana 63, 201–216.

Barboza-Gudiño, J.R., Ocampo-Díaz, Y.Z.E., Zavala-Monsiváis, A., López-Doncel, R.A., 2014. Procedencia como herramienta para subdivisión estratigráfica del Mesozoico temprano en el noreste de México. Revista Mexicana de Ciencias Geológicas 31 (3), 303–324.

Barboza-Gudiño, J.R., Ocampo-Díaz, Y.Z.E., Martínez, E., Loyola-Martínez, E., Pérez-Casillas, I.G., 2015. The Huizachal group in northeastern Mexico: a back-arc succession related to evolution of the early Jurassic Nazas arc. Cordilleran section. Geological Society of America 11th Annual Meeting, Alaska, Geological Society of America 47 (4), 55.

Bassett, K., Busby, C., 2005. Tectonic setting of the glance conglomerate along the Sawmill canyon fault zone, southern Arizona: a sequence analysis of an intra-arc strike-slip basin. In: In: Anderson, T.H., Nourse, J.A., McKee, J.W., Steiner, M.B. (Eds.), The Mojave-Sonora Megashear Hypotisis: Development, Assessment, and Alternatives 393. Geological Society of America, Special Paper, pp. 377–400.

Basu, A., Young, S.W., Suttner, L.J., James, W.C., Mack, G.H., 1975. Re-evaluation of the use of undulatory extinction and polycrystallinity in detrital quartz for provenance interpretation. J. Sediment. Petrol. 45, 873–882.

Bernet, M., Bassett, K., 2005. Provenance analysis by single-quartz-Grain SEM-CL/Optical microscopy. J. Sediment. Res. 75, 492–500.

Bhatia, M.R., Crook, A.W., 1986. Trace element characteristics of graywackes and tectonic setting discrimination of sedimentary basins. Contrib. Mineral. Petrol. 92, 181–193.

Boggs, S., Krinsley, D., 2006. Application to Cathodoluminescence Imaging to the Study of Sedimentary Rocks. Cambridge University Press, Cambridge, UK. https://doi.org/10.1017/CBO9780511535475.

Boschman, L., Molina-Garza, R.S., Langereis, C.G., van Hinsbergen, D.J.J., 2018. Paleomagnetic constraints on the kinematic relationship between the Guerrero terrane (Mexico) and North America since Early Cretaceous time. Geol. Soc. Am. Bull. 130 (7/8), 1131–1142. https://doi.org/10.1130/B31916.1.

Busby, C., 2012. Extensional and transtensional continental arc basins: case studies from the southwestern United States. In: Busby, C., Azor, A. (Eds.), Tectonics of Sedimentary Basins: Recent Advances. Wiley-Blacwell, pp. 382–404.

Celestino, U.J.L., 1982. Prospecto Alamitos, estudio geológico de detalle. Petróleos Mexicanos, Zona Norte. Informe Geológico(629) unpublished.

Centeno-García, E., 2017. Mesozoic tectono-magmatic evolution of Mexico: An overview. Ore Geol. Rev. 81, 1035–1052. https://doi.org/10.1016/j.oregeorev.2016.10.010.

Condie, K.C., 1993. Chemical composition and evolution of the Upper Continental Crust; contrasting results from surface samples and shales. Chem. Geol. 104, 1–37. https://doi.org/10.1016/0009-2541(93)90140-E.

Condie, K.C., Wronkiewicz, D.J., 1990. The Cr/Th ratio in Precambrian pelites from Kaapvaal craton as an index of craton evolution. Earth Planet. Sci. Lett. 97, 256–267.

Coney, P.J., 1983. Un modelo tectónico de México y sus relaciones con América del Norte, América del Sur y el Caribe. Revista del instituto Mexicano del Petróleo XV 1, 6–15.

Cox, R., Lowe, D.R., Cullers, R.L., 1995. The influence of sediment recycling and basement composition on evolution of mudrock chemistry in the southwestern United States. Geochimica et Cosmochimica Acta 59, 2919–2940. https://doi.org/10.1016/0016-7037(95)00185-9.

Cruz-Gámez, M.E., Velasco-Tapía, F., Ramírez-Fernández, J.A., Jenchen, U., Rodríguez-Saavedra, P., Rodríguez-Díaz, A.A., Iriondo, A., 2017. Volcanic sequence in Late Triassic-Jurassic siliciclastic and evaporitic rocks from Galeana, NE Mexico. Geologica Acta 15 (2), 89–106. https://doi.org/10.1344/GeologicaActa2017.15.2.2.

Dalrymple, R.W., 2010. Tidal depositional systems. In: James, N.P., Dalrymple, R.W. (Eds.), Facies Models 4. GeoText 6. The Geological Association of Canada, pp. 201–231.

Dercourt, J.R., Luc, E., Vrielynck, B., Insitut Français du Pétrole, 1993. Atlas Tethys palaeonvironmental maps. Gauthier-Villars: Diffusion-CCGM, Paris, pp. 307 p.

Dickinson, W.R., 1970. Interpreting detrital modes of graywacke and arkose. J. Sediment. Res. 40, 695–707. https://doi.org/10.1306/74D72018-2B21-11D7-8648000102C1865D.

Dickinson, W.R., Lawton, T.F., 2001. Carboniferous to Cretaceous assembly and fragmentation of Mexico. Geol. Soc. Am. Bull. 113 (9), 1142–1160. https://doi.org/10.1130/0016-7606(2001)113<1142:CTCAAF>2.0.CO;2.

Dickinson, W.R., Suczek, C.A., 1979. Plate tectonics and sandstone compositions. Am. Assoc. Pet. Geol. Bull. 63, 2164–2182.

Elías-Herrera, M., Sánchez-Zavala, J.L., Macias-Romo, C., 2000. Geologic and geochronologic data from the Guerrero terrane in the Tejupilco area, southern Mexico: new constraints on its tectonic interpretation. J. South Am. Earth Sci. 13, 355–375.

Fastovsky, D.E., Hermes, O.D., Strater, N.H., Bowring, S.A., Clark, J.M., Montellano, M., Hernandez, R., 2005. Pre–Late Jurassic, fossil-bearing volcanic and sedimentary red beds of Huizachal canyon, Tamaulipas, Mexico. In: In: Anderson, T.H., Nourse, J.A., McKee, J.W., Steiner, M.B. (Eds.), The Mojave-Sonora Megashear Hypothesis: Development, Assessment, and Alternatives 393. Geological Society of America, Special Paper, pp. 401–426. https://doi.org/10.1130/0-8137-2393-0.401.

Fedo, C.M., Nesbitt, H.W., Young, G.M., 1995. Unraveling the effects of potassium metasomatism in sedimentary rocks and paleosols, with implications for paleoweathering conditions and provenance. Geology 23, 921–924. https://doi.org/10.1130/0091-7613(1995)023<0921:UTEOPM>2.3.CO;2.

Fillon, R.H., 2007. Mesozoic Gulf of Mexico basin evolution from a planetary perspective and petroleum system implications. Pet. Geosci. 13, 105–126. https://doi.org/10.1144/1354-079307-745.

García-Díaz, J.L., 2004. Etude Géologique de la Sierra Madre del sur aux environs de Chilpancingo et D'Olinala, Gro: Une contribution à la connaissance de l'évolution géodynamique de la marge pacifique du Mexique depuis le Jurassique. Ph.D Thesis. Université de Savoie, Chambery, pp. pp. 148.

Garzanti, E., 2016. From static to dynamic provenance analysis—sedimentary petrology upgraded. Sediment. Geol. 336, 3–13. https://doi.org/10.1016/j.sedgeo.2015.07.010.

Gazzi, P., 1966. Le arenarie del flysch sopracretaceo dell'Appennino modenese; Correlazioni con il flysch di Monghidoro. Mineral et Petrographicha Acta 12, 67–97.

Godínez-Urban, A., Lawton, T.F., Molina Garza, R.S., Iriondo, A., Weber, B., López-Martínez, M., 2011a. Jurassic volcanic and sedimentary rocks of the La Silla and Todos Santos Formations, Chiapas: record of Nazas arc magmatism and rift-basin formation prior to opening of the Gulf of Mexico. Geosphere 7, 121–144.

Godínez-Urban, A., Molina-Garza, R.S., Geissman, J.W., Wawrzyniec, T., 2011b. Paleomagnetism of the todos santos and La silla formations, Chiapas: implications for the opening of the Gulf of Mexico. Geosphere 7, 145–158. https://doi.org/10.1130/GES00604.1.

Goldhammer, R.K., 1999. Mesozoic sequence stratigraphy and paleogeographic evolution of northeast Mexico. In: Bartolini, C., Wilson, J.L., Lawton, T.F. (Eds.), Mesozoic Sedimentary and Tectonic History of North-Central Mexico, pp. 1–58 Geological Society of America, Special Paper 340.

Gose, W.A., Belcher, R.C., Scott, G.R., 1982. Paleomagnetic results from northeastern Mexico: evidence for large Mesozoic rotations. Geology 10, 50–54. https://doi.org/10.1130/0091-7613(1982)10<50:PRFNME>2.0.CO;2.

Götze, J., Zimmerle, W., 2000. Quartz and silica as guide to provenance in sediments and sedimentary rocks. Contrib. Sediment. Geol. 21, 1–91.

Haenggi, W.T., 2002. Tectonic history of the chihuahua trough, Mexico and adjacent USA, part II: mesozoic and cenozoic. Boletín de la Sociedad Geológica Mexicana, LV 1, 38–94.

Herron, M.M., 1988. Geochemical classification of terrigenous sands and shales from core of log data. J. Sediment. Petrol. 58 (5), 820–829.

Korte, C., Hesselbo, S.P., Ulmann, C.V., Dietl, G., Ruhl, M., Scweigert, G., Thibault, N., 2015. Jurassic climate mode governed by ocean gateway. Nat. Commun. 6, 10015. https://doi.org/10.1038/ncomms10015.

Labarthe, H.G., Tristán-González, M., Aguillón-Robles, A., Jiménez-López, L.S., 1989. Cartografía Geológica 1: 50,000 de las hojas El Refugio y Mineral El Realito, Estados de San Luis Potosí y Guanajuato. Universidad Autónoma de San Luis Potosí, Instituto de Geología, San Luis Potosí, México.

Lawton, T.F., Molina-Garza, R.S., 2014. U-Pb geochronology of the type Nazas Formation and superjacent strata, northeastern Durango, Mexico: implication of a Jurassic age

for continental-arc magmatism in north-central Mexico. Geol. Soc. Am. Bull. 126 (-10), 1181–1199. https://doi.org/10.1130/B30827.1.

Lawton, F.T., Juárez-Arriaga, E., Ocampo-Díaz, Y.Z.E., Beltrán-Treviño, A., Martens, U., Stockli, D.F., 2016. Evolution of late cretaceous-paleogene foreland sediment-dispersal systems of Northern and Central Mexico. In: Lowry, C.M., Snedden, J.W., Rosen, N.C. (Eds.), Mesozoic of the Gulf Rim and Beyond: New Progress in Science and Exploration of the Gulf of Mexico Basin. Houston, TX, USA, Gulf Coast Section SEPM (GCSSEPM), pp. 283–308.

Lesnov, F.P., 2010. Rare Earth Elements in Ultramafic and Mafic Rocks and Their Minerals: Main Types of Rocks. Rock-forming Minerals. CRC press, pp. pp.324.

Loyola, M.E., 2015. Datos para la reconstrucción paleoclimática del Jurásico Inferior a Medio en la Mesa Central de México. Unpublished Master Sciences Thesis. Universidad Autónoma de San Luis Potosí, pp. 82 pp..

Marsaglia, K.M., Tazaki, K., 1992. Diagenetic trends in ODP Leg 126 sandstones. In: In: Taylor, B., Fujioka, K. (Eds.), Proceeding of the Ocean Drilling Program, Scientific Results, College Station,TX (Ocean Drilling Program) 126. pp. 125–138.

Martini, M., Ortega-Gutiérrez, F., 2018. Tectono-stratigraphic evolution of eastern Mexico during the break-up of Pangea: A review. Earth. Rev. 183, 38–55. https://doi.org/10.1016/j.earscirev.2016.06.013.

Marton, G.L., 1995. Jurassic Evolution of the Southeastern Gulf of Mexico. ph.d Thesis. The University of Texas at Austin, United States, pp. pp. 276.

McLennan, S.M., Hemming, S., McDaniel, D.K., Hanson, G.N., 1993. Geochemical approaches to sedimentation, provenance and tectonics. In: In: Johnsson, M.J., Basu, A. (Eds.), Processes Controlling the Composition of Clastic Sediments. 284. Geological Society of America, Special Paper, pp. 21–40.

Michalzik, D., Shumann, D., 1994. Lithofacies relations and paleoecology of a Late Jurassic to Early Cretaceous Fan Delta to Shelf depositional system in the Sierra Madre Oriental of North-East Mexico. Sedimentology 41, 463–477. https://doi.org/10.1111/j.1365-3091.1994.tb02006.x.

Molina-Garza, R.S., Van Der Voo, R.O.B., Urrutia-Fucugauchi, J., 1992. Paleomagnetism of the Chiapas Massif, southern Mexico: evidence for rotation of the maya block and implications for the opening of the Gulf of Mexico. Geol. Soc. Am. Bull. 104, 1156–1168. https://doi.org/10.1130/0016-7606(1992)104<1156:POTCMS>2.3.CO;2.

Nesbitt, H.W., Young, G.M., 1982. Early Proterozoic climates and plate motions inferred from major element chemistry of lutites. Nature 299, 715–717.

Ocampo-Díaz, Y.Z.E., 2011. Implicaciones Tectono-sedimentarias de las intercalaciones clásticas en el límite Jurásico-Cretácico del Noreste de México (Fosa de Monterrey y Cuenca de Sabinas). Ph.D.Thesis. Universidad Autónoma de Nuevo León, Nuevo León, México, pp. pp. 275.

Ocampo-Díaz, Y.Z.E., Rubio-Cisneros, I.I., 2013. Reciclamiento sedimentario: Análisis composicional asociado a discordancias del noroeste de México, un ejemplo del Triásico Superior al Cretácico Inferior. Boletín de la Sociedad Geológica Mexicana 65, 553–572.

Ocampo-Díaz, Y.Z.E., Talavera-Mendoza, O., Jenchen, U., Valencia, V.A., Medina-Ferrusquia, H.C., Guerrero-Suastegui, M., 2014. Procedencia de la Formación La Casita y la Arcosa Patula: implicaciones para la evolución tectono-magmática del NE de México entre el Carbonífero y el Jurásico. Revista Mexicana de Ciencias Geológicas 31, 45–63.

Ohta, T., Arai, H., 2007. Statistical empirical index of chemical weathering in igneous rocks: a new tool for evaluating the degree of weathering. Chem. Geol. 240, 280–297. https://doi.org/10.1016/j.chemgeo.2007.02.017.

Ortega-Flores, B., Solari, L., Lawton, T.F., Ortega-Obregón, C., 2014. Detrital-zircon record of major Middle Triassic-Early Cretaceous provenance shift, central Mexico: demise of Gondwana continental fluvial systems and onset of back-arc volcanism and sedimentation. Int. Geol. Rev. 56 (2), 237–261.

Ortega-Flores, B., Solari, L.A., Escalona-Alcázar, F.J., 2016. The Mesozoic successions of western Sierra de Zacatecas, Central Mexico: provenance and tectonic implications. Geol. Mag. 153 (4), 1–22. https://doi.org/10.1017/S0016756815000977.

Ortega-Gutiérrez, F., Elías-Herrera, M., Morán-Zenteno, D.J., Solari, L., Weber, B., Luna-González, L., 2018. The pre-Mesozoic metamorphic basement of Mexico, 1.5 billion years of crustal evolution. Earth Sci. Rev. 183, 2–37. https://doi.org/10.1016/j.earscirev.2018.03.006.

Peña-Alonso, T.A., Molina-Garza, R.S., Villalobos-Escobar, G., Estrada-Carmona, J., Levresse, G., Solari, L., 2018. The opening and closure of the Jurassic-Cretaceous Xolapa basin, southern Mexico. J. South Am. Earth Sci. 88, 599–620. https://doi.org/10.1016/j.jsames.2018.10.003.

Pindell, J.L., 1985. Alleghenian reconstruction and subsequent evolution of the Gulf of Mexico, Bahamas, and Proto-Caribbean. Tectonics 4 (1), 1–39. https://doi.org/10.1029/TC004i001p00001.

Pindell, J.L., Kennan, L., 2009. Tectonic evolution of the Gulf of Mexico, Caribbean and northern South America in the mantle reference frame: an update. In: In: James, K.H., Lorente, M.A., Pindell, J.L. (Eds.), The Origin and Evolution of the Caribbean Plate 328. Geological Society of London, London, Special Publication, pp. 1–55. https://doi.org/10.1144/SP328.1.

Rosaz, T., 1989. Les passage des Cordilléres Nord-Américaines aux Sierras Madres Mexicaines le long du Texas Lineament Géologie du SW du Nouveau-Mexique (USA). Bulletin des Centre de Recherches Exploration-Production Elf-Aquitaine 13 (2), 247–275.

Rubio-Cisneros, I.I., Lawton, T.F., 2011. Detrital zircon U-Pb ages of sandstones in continental red beds at Valle de Huizachal, Tamaulipas, NE Mexico: record of Early-Middle Jurassic arc volcanism and transition to crustal extension. Geosphere 7 (1), 1–12. https://doi.org/10.1130/GES00567.1.

Taylor, S.R., McLennan, S.M., 1985. The Continental Crust: Its Composition and Evolution. Blackwell, Oxford, pp. pp. 312.

Torres Sánchez, S.A., Augustsson, C., Barboza Gudiño, J.R., Jenchen, U., Ramírez Fernández, J.A., Abratis, M., Scherstén, A., 2016. Magmatic source and metamorphic grade of metamorphic rocks from the Granjeno Schist: was northeastern Mexico a part of Pangaea? Geol. J. 51, 845–863. https://doi.org/10.1002/gj.2702.

Torres-Sánchez, S.A., Augustsson, C., Jenchen, U., Barboza-Gudiño, J.R., Abratis, M., Torres-Sánchez, D., Ramírez Fernández, J.A., 2017. Petrology and geochemistry of metaultramafic rocks in the Paleozoic Granjeno Schist, northeastern Mexico: remnants of Pangaea ocean floor. Open Geosci. 9, 361–384. https://doi.org/10.1515/geo-2017-0029.

Tortosa, A., Palomares, M., Arribas, J., 1991. Quartz grain types in Holocene deposits from the Spanish Central system: some problems in provenance analysis. In: In: Morton, A.C., Todd, S.P., Haughton, P.D.W. (Eds.), Developments in Provenance Studies 57. Geological Society, London, Special Publication, pp. 47–54. https://doi.org/10.1144/GSL.SP.1991.057.01.05.

Venegas-Rodríguez, G., Barboza-Gudiño, J.R., López-Doncel, R.A., 2009. Geocronología de circones detríticos en capas del Jurásico Inferior de las áreas de la Sierra de Catorce y El Alamito en el estado de San Luis Potosí. Revista Mexicana de Ciencias Geológicas 26, 466–481.

Walker, R., 1992. Turbidites and submarine fans. In: Walker, R., James, N.P. (Eds.), Facies Models: Response to Sea Level Change, GEOText1. The Geological Association of Canada, pp. 239–263.

Weber, B., Scherer, E.E., Schulze, C., Valencia, V.A., Montecinos, P., Metzger, K., Ruiz, J., 2010. U-Pb and Lu-Hf isotope systematics of lower crust from central-southern Mexico – geodynamic significance of Oaxaquia in a Rodinia Realm. Precambrian Geol. 182, 149–162. https://doi.org/10.1016/j.precamres.2010.07.007.

Weltje, G.J., 2002. Quantitative analysis of detrital modes: statistically rigorous confidence regions in ternary diagrams and their use in sedimentary petrology. Earth Sci. Rev. 57, 211–253. https://doi.org/10.1016/S0012-8252(01)00076-9.

White, T., Witzke, B., Ludvigson, G., Brenner, R., 2005. Distinguishing base-level change and climate signals in a Cretaceous alluvial sequence. Geology 33, 13–16. https://doi.org/10.1130/G20995.1.

Winker, C.D., Buffler, R.T., 1988. Paleogeographic evolution of early deep-water Gulf of Mexico and margins, Jurassic to Middle Cretaceous (Comanchean). Am. Assoc. Pet. Geol. Bull. 72, 318–346.

Zepeda-Martínez, M., Martini, M., Solari, L., 2018. A major provenance changes in sandstones from the Tozoatlán basin, southern Mexico, controlled by Jurassic, sinistral normal motion along the Salado River fault: implication for the reconstruction of Pangea. J. South Am. Earth Sci. 86, 447–460. https://doi.org/10.1016/j.jsames.2018.07.008.

Zinkernagel, U., 1978. Cathodoluminescence of quartz and its application to sandstone petrology. Contrib. Sediment. 8, 1–69.

Zuffa, G.G., 1980. Hybrid arenites; their composition and classification. J. Sediment. Res. 50, 21–29.